THE JOURNAL OF BIOLOGICAL CHEMISTRY VOL. 285, NO. 43, pp. 33265–33280, October 22, 2010

Mammalian Tropomodulins Nucleate Actin Polymerization via Their Actin Monomer Binding and Filament Pointed End-capping Activities*[S]

Received for publication, May 14, 2010, and in revised form, June 18, 2010 Published, JBC Papers in Press, July 21, 2010, DOI 10.1074/jbc.M110.144873

Sawako Yamashiro[‡1], **Kaye D. Speicher**[§], **David W. Speicher**[§], **and Velia M. Fowler**[‡2]

From the [‡]*Department of Cell Biology, The Scripps Research Institute, La Jolla, California 92037 and the* [§]*Center for Systems and Computational Biology, The Wistar Institute, Philadelphia, Pennsylvania 19104*

Many actin-binding proteins have been shown to possess multiple activities to regulate filament dynamics. Tropomodulins (Tmod1–4) are a conserved family of actin filament pointed end-capping proteins. Our previous work has demonstrated that Tmod3 binds to monomeric actin in addition to capping pointed ends. Here, we show a novel actin-nucleating activity in mammalian Tmods. Comparison of Tmod isoforms revealed that Tmod1–3 but not Tmod4 nucleate actin filament assembly. All Tmods bind to monomeric actin, and Tmod3 forms a 1:1 complex with actin. By truncation and mutagenesis studies, we demonstrated that the second α-helix in the N-terminal domain of Tmod3 is essential for actin monomer binding. Chemical cross-linking and LC-MS/MS further indicated that residues in this second α-helix interact with actin subdomain 2, whereas Tmod3 N-terminal domain peptides distal to this α-helix interact with actin subdomain 1. Mutagenesis of Leu-73 to Asp, which disrupts the second α-helix of Tmod3, decreases both its actin monomer-binding and -nucleating activities. On the other hand, point mutations of residues in the C-terminal leucine-rich repeat domain of Tmod3 (Lys-317 in the fifth leucine-rich repeat β-sheet and Lys-344 or Arg-345/Arg-346 in the C-terminal α6-helix) significantly reduced pointed end-capping and nucleation without altering actin monomer binding. Taken together, our data indicate that Tmod3 binds actin monomers over an extended interface and that nucleating activity depends on actin monomer binding and pointed end-capping activities, contributed by N- and C-terminal domains of Tmod3, respectively. Tmod3 nucleation of actin assembly may regulate the cytoskeleton in dynamic cellular contexts.

Dynamic assembly and disassembly of actin filaments are essential for establishing functional actin networks to execute various cellular phenomena. Regulation of actin dynamics at the filament ends, where polymerization and depolymerization occur, is crucial for rearrangement of the actin cytoskeleton. Although the concentration of monomeric actin in cells is in excess of the critical concentrations for assembly at both barbed and pointed ends, actin polymerization occurs predominantly at fast growing barbed ends (1, 2). Indeed, the actin barbed end-binding drug cytochalasin D inhibits many cellular phenomena, including cell migration, cell adhesion, and endocytosis (3–5). Six actin-nucleating proteins, including Arp2/3, formins, spire, cordon-bleu, leiomodin 2 (Lmod2), and JMY, have been described and play important roles in enhancing actin polymerization from barbed ends of filaments *in vivo* (6–11). It appears that each of these proteins has a unique mechanism for actin nucleation. Arp2 and Arp3 subunits of the Arp2/3 complex are thought to template a new actin filament from the side of a preexisting filament and to anchor the pointed end of the growing filament (12). Formin homology 2 domains of formin family proteins form homodimers and stabilize an actin dimer that resembles the actin short pitch dimer in the filament model, suggesting a distinct templating mechanism (13). Spire, cordon-bleu, and JMY contain tandem G-actin-binding WH2 motifs, thereby tethering multiple actin molecules into an oligomer that acts as a nucleus (8–10). Leiomodin2 (Lmod2), a member of the tropomodulin (Tmod)[3] actin filament pointed end capping protein family, shares the domain organization of Tmods but contains a C-terminal extension of ~150 amino acids that includes an actin-binding WH2 domain (11, 14). Lmod2 is a potent nucleator of actin polymerization, and both the Tmod-related and WH2 domains are necessary for this activity (11). In addition to these actin-nucleating proteins, a recent study has demonstrated that vinculin is capable of nucleating actin assembly in low ionic strength buffer conditions, but the mechanism of actin nucleation by vinculin and its physiological significance are unclear (15). The diversity of the mechanisms among these proteins demonstrates that independently evolved proteins have developed distinct ways of achieving the important nucleation function, which are presumably optimized for controlling actin networks in various cellular situations.

Tmods are a conserved family of actin filament pointed end-capping proteins. There are four Tmod isoforms (Tmod1–4), each of which is expressed in a tissue-specific fashion (16).

* This work was supported, in whole or in part, by National Institutes of Health Grants HL083464 (to V. M. F.) and HL038794 (to D. W. S.).

[S] The on-line version of this article (available at http://www.jbc.org) contains supplemental Tables I–III and Figs. S1–S6.

[1] To whom correspondence may be addressed: Dept. of Cell Biology, CB163, The Scripps Research Institute, 10550 N. Torrey Pines Road, La Jolla, CA 92037. Tel.: 858-784-8277; Fax: 858-784-8753; E-mail: syamash@scripps.edu.

[2] To whom correspondence may be addressed: Dept. of Cell Biology, CB163, The Scripps Research Institute, 10550 N. Torrey Pines Road, La Jolla, CA 92037. Tel.: 858-784-8277; Fax: 858-784-8753; E-mail: velia@scripps.edu.

[3] The abbreviations used are: Tmod, tropomodulin; LRR, leucine-rich repeat; EDC, 1-ethyl-2-(3-dimethylaminopropyl)-carbodiimide; sulfo-NHS, sulfo-*N*-hydroxylsulfosuccinimide; BisTris, 2-[bis(2-hydroxyethyl)amino]-2-(hydroxymethyl)propane-1,3-diol; Bicine, *N*,*N*-bis(2-hydroxyethyl)glycine.

Tmod1, which has been studied most extensively, and Tmod3 are expressed in a wide variety of tissues, whereas expression of Tmod2 and Tmod4 is restricted to neuronal tissues and skeletal muscle, respectively (14, 16–18). Tmods cap the pointed ends of actin filaments (19, 20) and also bind to tropomyosin and cap pointed ends of tropomyosin-decorated actin filaments with an affinity more than 1000-fold greater than for bare pointed ends (19, 20). *In vivo*, Tmods play critical roles in regulating actin dynamics in a wide variety of cytoskeletal structures that are each uniquely modulated (16). Tmod1 is best known for promoting actin filament assembly and regulating filament lengths in myofibrils of striated muscles (21–24). More recent studies show that Tmod1 also controls actin filament lengths and stability in the spectrin-based membrane skeletons of lens fiber cells (25) and red blood cells (68). Tmod3 is associated with lateral membranes of polarized epithelial cells where it stabilizes actin filaments and maintains cell height (26). Tmod3 is also associated with dynamic actin filaments in the leading lamellipodia and ruffles of migrating endothelial cells, where it negatively regulates rates of cell migration (27). However, the actin filament pointed end-capping activity of Tmods, which is their best characterized property, may be insufficient to interpret these various experimental phenotypes.

Tmods contain two distinct major domains (see Fig. 5*A*) (16). First, the unstructured N-terminal domain contains three functional α-helices and caps the pointed ends of tropomyosin-decorated actin filaments(Fig. 5*A*) (20, 28, 29). The first α-helix in the chicken Tmod1 N-terminal domain (residues 24–35) has been experimentally identified by NMR spectroscopy (28). The second (residues 65–75 in chicken Tmod1) and third (residues 126–135 in chicken Tmod1) α-helices have been identified by secondary structure prediction analysis (29, 30). The first and third α-helices bind to tropomyosin (28, 29), and the second α-helix is suggested to cap actin filament pointed ends in a tropomyosin-dependent manner, based on elimination of these functionalities by predicted α-helix disrupting mutations (28, 30). The N-terminal domain of Tmod3 can also bind to monomeric actin and sequester it from polymerization (31). However, Tmod3 contains no sequence similarities to any known actin monomer-binding proteins, including the WH2 domain, actin-depolymerizing factor-homology domain, profilin domain, and the actin monomer-binding linker found in JMY and spire (9, 32). Therefore, how Tmod3 binds to actin is still unclear, as is the relationship of monomer binding to tropomyosin binding or actin capping, and to Tmod functions *in vivo*.

Second, the C-terminal half of Tmods is compact, folded, and composed of a series of leucine-rich repeats (LRRs) with an associated C-terminal α-helix (α6) that contains a tropomyosin-independent actin pointed end-capping activity (Fig. 5*A*) (20). Our previous study demonstrated that the α6-helix is critical for tropomyosin-independent actin pointed end-capping by chicken Tmod1 (20). However, which residues in the C-terminal domain of Tmod are essential for pointed end capping remains unclear. In addition to these activities, our previous studies have shown that chicken Tmod1 and human Tmod3 can promote actin assembly with different efficiencies *in vitro*, suggesting that Tmods may have actin-nucleating activity (20, 31). However, which domains are responsible and how Tmods promote actin polymerization have not yet been investigated.

In this study, we show that mammalian Tmod1–3 nucleate actin filament assembly. By characterizing truncated fragments and point mutations of Tmod3, we found that the actin-nucleating activity of Tmods depended on two distinct actin-binding activities. The first is actin monomer-binding activity, conferred by α-helix2 in the N-terminal domain, which is conserved among all Tmod isoforms that we tested. The second is actin pointed end-capping activity, conferred by the β-sheet of the fifth LRR and α6-helix in the C-terminal domain, which is conserved among Tmod1, Tmod3, and Tmod4 (20, 27). These biochemical results suggest a mechanistic model for actin nucleation by Tmods and provide new insights into the interaction between the N- and C-terminal domains of Tmods with the pointed end of actin monomers and filaments.

EXPERIMENTAL PROCEDURES

Construction of cDNAs and Expression of Recombinant Tmod Proteins—Full-length mouse Tmod3 and Tmod4 were inserted in-frame in the pGEX-KG vector so as to code for a fusion protein with glutathione *S*-transferase (GST) on the N-terminal end of Tmod3 and Tmod4. Site-specific mutations were generated by the two-step PCR protocol (33) or a QuikChange™ mutagenesis kit (Stratagene) using pGEX-KG-mouse Tmod3 as a template. cDNAs encoding GST fusion proteins with various Tmod3 fragments were inserted in the BamHI and EcoRI sites in the linker region of the pGEX-KG vector using the PCR with appropriate primers and pGEX-KG mouse Tmod3 as a template. The primers used are shown in supplemental Table 1. The entire Tmod3 and Tmod4 coding region of each plasmid was sequenced to confirm the presence of introduced mutations and the absence of PCR-induced errors. GST fusion Tmod3 and Tmod4, mutant Tmod3, and Tmod3 fragments were expressed in BL21 *Escherichia coli* and purified as described previously (20, 34). Protein concentrations were determined spectroscopically as described in Table 1 or by using a BCA protein assay kit (Pierce).

Proteins—Rabbit skeletal muscle actin was prepared from acetone powder as described previously (35). Pyrene-labeled actin was prepared and stored as described previously (36). Prior to use in assays, actin was dialyzed several times against freshly prepared buffer A (2 mM Tris, pH 8.0, 0.2 mM $CaCl_2$, 0.2 mM ATP, 1 mM DTT) and then centrifuged for 1 h at 148,000 × *g* to remove minor amounts of aggregated material. Gelsolin was a gift from J. Bryan (Baylor College of Medicine, Dallas, TX) and was prepared as described previously (37). Protein concentrations were determined for actin and gelsolin by absorption at 290 or 280 nm with E_{290} = 24.9 mM^{-1} cm^{-1} and E_{280} = 150 mM^{-1} cm^{-1}, respectively (19).

Fluorescence Assays for Actin Polymerization—To measure actin nucleation, 4 μM of G-actin (8% pyrenyl) was converted to Mg^{2+}-actin as described previously (38), and then the indicated concentrations of Tmod1–4, Tmod3 fragments, or mutant Tmod3 were added and incubated for 1 min. Polymerization was then initiated by the addition of one-tenth volume of 10× polymerizing buffer (200 mM Hepes, pH 7.5, 1 M KCl, 20 mM $MgCl_2$, 2 mM DTT, 5 mM ATP, 10 mM EGTA). Fluorescence

measurements (excitation = 366.5 nm and emission = 407 nm) were made using a Fluoromax 3 fluorimeter (Jobin Yvon, Edison, NJ). To assay for barbed end elongation, 0.6 μM G-actin (8% pyrenyl) was polymerized in the presence or absence of 50 nM Tmod3 or 5 nM cytochalasin D. The concentration of barbed ends was calculated from the elongation rate (measured by the rate of polymerization, where 50% of monomers were polymerized) as described previously (20, 39).

Measurements of elongation rates at the pointed end were performed using 2.5 μM G-actin (8% pyrenyl) and 10 nM gelsolin-capped actin filaments (gelsolin/actin, 1:10) as nuclei for polymerization as described previously (19, 20). Capping activity for Tmod3 wild type, mutant proteins, and fragments were obtained from the initial elongation rates, measured directly from the slopes of the polymerization traces over the first 1 min. Rates in the presence of increasing concentrations of Tmod (100 nM to 1 μM) were divided by the rate for actin in the absence of Tmod, giving a rate/control rate. The theoretical elongation rates were calculated using the two equations to describe Tmod3 binding to actin monomers (Equation 1) and to describe the rate of actin elongation at pointed ends (Equation 2), where K_+ is the rate constant for association of ATP-actin subunits at the pointed end = 1.3 $\mu M^{-1}\ s^{-1}$ (39).

$$K_d \text{ for Tmod3 binding to G-actin} = ([\text{G-actin}]_{tot} - [\text{G-actin} - \text{Tmod3}])([\text{Tmod3}]_{tot} - [\text{G-actin:Tmod3}])/[\text{G-actin:Tmod3}] \quad \text{(Eq. 1)}$$

$$\text{rate of polymerization} = [\text{pointed ends}][K_+ \cdot [\text{G-actin}]] \quad \text{(Eq. 2)}$$

Assuming that Tmod3 possesses only G-actin-binding and -sequestering activities, we calculated a theoretical pointed end elongation rate as follows. First, the concentrations of the G-actin-Tmod3 complex were calculated using Equation 1, where the K_d for Tmod3-actin monomer binding was K_d = 0.51 μM (31), total G-actin = 2.5 μM, and total Tmod3 = 100 nM to 1 μM as described above. The rate of polymerization in each assay was then calculated using Equation 2, where [pointed ends] = 10 nM (the concentration of the pointed ends of gelsolin-capped actin seeds in this assay), K_+ = 1.3 μM (39), and [G-actin] = total [G-actin] (2.5 μM) − [G-actin-Tmod3 complex]. Because the concentration of pointed ends (10 nM) and the association rate of actin for pointed ends (1.3 μM) are stable in Equation 2, the theoretical rate of polymerization is in direct proportion to [G-actin] if Tmod3 does not cap the pointed end.

Actin Cross-linking Assays—Cross-linking of G-actin and Tmod3 was performed as described previously (31) with slight modifications. Briefly, G-actin and wild-type or mutant Tmod3 were exchanged into a buffer containing 5 mM Hepes, pH 7.5, and 0.1 mM $CaCl_2$ using Zeba Spin Desalting Columns (Pierce). G-actin and Tmod3 were combined at a 1:1 molar ratio at 10 μM each and then incubated for 20 min with 1 mM of EDC (Pierce) and 1 mM of sulfo-NHS (Pierce) at room temperature. Following addition of 10 mM hydroxylamine to stop the reaction, samples were separated by SDS-PAGE (40) using various percent acrylamide as indicated in figures. Gels were stained with Coomassie Brilliant Blue R-250 (Sigma).

Nondenaturing PAGE—Nondenaturing PAGE was performed as described by Safer (41). G-actin and Tmod1–4, Tmod3 fragments, or Tmod3 mutants at indicated concentrations were incubated in buffer A for 20 min at room temperature. The samples were then supplemented with 0.25 volume of a loading buffer (50% glycerol, 0.05% bromphenol blue) and electrophoresed using a Bicine/triethanolamine buffer system. The proteins were visualized by staining with Coomassie Brilliant Blue R-250.

Gel Filtration Assays—G-actin alone, Tmod3 alone, or the mixture of G-actin and Tmod3 at indicated concentrations were incubated in buffer A for 20 min on ice and then centrifuged for 20 min at 285,000 × *g* to remove aggregates. The samples were characterized by a Superdex 200HR 10/30 column (GE Healthcare) in buffer A. The elution profiles were determined from absorption at 280 nm using a Monitor UV-900 (GE Healthcare). In each assay, 0.5-ml fractions were collected and subjected to SDS-PAGE.

In-gel Trypsin Digestion and LC-MS/MS—The cross-linking reaction between G-actin and Tmod3 or Tmod3-(43–189) fragment was performed as described above. Reaction mixtures were separated on 10% BisTris NuPAGE gels (Invitrogen) with MOPS running buffer (Invitrogen), and gels were stained with colloidal blue staining kit (Invitrogen). The bands of interest were excised and digested in gel as described previously (42) using modified trypsin (Promega). Locations of cross-linked residues were determined using LC-MS/MS on an LTQ Orbitrap XL mass spectrometer (Thermo Fisher Scientific), equipped with a NanoLC™ pump and autosampler (Eksigent Technologies). Tryptic peptides were separated by RP-HPLC on a PicoFrit® (New Objective) 75-μm inner diameter × 15-cm nanocapillary column packed with 5 μm of MAGIC C18 resin (Michrom BioResources). Solvent A was 0.1% formic acid in Milli-Q® water (Millipore), and solvent B was 0.1% formic acid in acetonitrile. Peptides were eluted at 300 nl/min using an acetonitrile gradient consisting of 3–28% solvent B over 40 min, 28–50% solvent B over 25.5 min, 50–80% solvent B over 5 min, and 80% solvent B for 5 min before returning to 3% solvent B in 2 min. The LTQ-Orbitrap mass spectrometer was set to perform a full MS scan (m/z 400–2000) in the Orbitrap at a resolution of 60,000 for the MS scan. The six most intense ions exceeding a minimum threshold of 1,000 were selected for MS/MS in the linear ion trap using an isolation width of 2.5 Da. Monoisotopic precursor selection was disabled, and singly- as well as doubly-charged ions were excluded from MS/MS analysis. Ions subjected to MS/MS were excluded from repeated analysis for 45 s.

Identification of Cross-linked Peptides—Cross-linked and noncross-linked control proteins were analyzed in parallel using LC-MS/MS. For data analysis, the LC-MS patterns for the control and cross-linked sample were compared using Rosetta Elucidator software (version 3.2) (Rosetta Biosoftware) to identify all features unique to the cross-linked sample. Features are discrete mass/charge (m/z) ions detected throughout the HPLC. MH^+ values for all remaining features that had a charge of >2 were then compared with the MH^+ for all theoretical

cross-linked peptides, which were calculated using either GPMAW version 8 or custom software written in-house, which served the same function as GPMAW but was more efficient. Ions specific to cross-linked samples and within 5 ppm of a theoretical cross-linked peptide were selected for further analysis. The Fuzzy Ions program in the SEQUEST Browser software (Thermo Fisher Scientific) and *de novo* sequencing were used to verify cross-linked peptides and to identify specific amino acid residue positions involved in the cross-links. In cases where the available MS/MS spectra could not distinguish between closely spaced candidate cross-link sites, all possible cross-link sites were indicated (see "Results").

RESULTS

Mammalian Tmods Promote Spontaneous Actin Polymerization—Our previous studies have shown that chicken Tmod1 promotes actin polymerization weakly at micromolar concentrations, whereas human Tmod3 enhances actin polymerization strongly at nanomolar concentrations (20, 31). To compare directly the effects of Tmod isoforms on actin polymerization, first we examined the kinetics of spontaneous actin polymerization in the presence of recombinant mammalian Tmod1–4 (Fig. 1*A*). In pyrenyl-actin polymerization assays, 50–400 nM Tmod1–3 accelerated 4 μM actin polymerization to similar extents (Fig. 1*A*). On the other hand, Tmod4 had no effect on spontaneous actin polymerization, even at concentrations up to 1 μM (Fig. 1*A* and data not shown). Because our previous studies showed that neither Tmod1 nor Tmod3 enhance actin elongation from free barbed or pointed ends of pre-formed actin seeds (19, 31), we concluded that the ability of Tmod1–3 to promote spontaneous polymerization was due to enhancement of filament nucleation.

Tmod1 and Tmod2 exhibited increasing actin-nucleating activity in a dose-dependent manner at the tested concentrations, and the effect of Tmod2 on actin polymerization was saturated at >200 nM (Fig. 1*A*). Although Tmod3 enhanced the initial rate of polymerization in a dose-dependent manner up to 200 nM, the rate of polymerization at 400 nM Tmod3 was somewhat less than at 200 nM (Fig. 1*A*), which can be attributed to the monomer-sequestering activity of Tmod3 that we demonstrated previously (also see below) (31). Although the lag phase of polymerization was shortened in the presence of Tmod1–3, it was not eliminated even at the highest concentrations tested. This suggests that Tmods promote actin assembly most likely by stabilizing spontaneously forming actin nuclei.

Next, we calculated the concentrations of actin filament free barbed ends in these assays (Fig. 1*B*). Note that actin assembles from barbed ends in the presence of Tmods as we describe in the next paragraph. We found that Tmod2 exhibited the strongest actin nucleation activity with 200–400 nM Tmod2 increasing the concentration of barbed ends up to 4–5-fold when compared with polymerization of actin alone. Tmod1 and Tmod3 showed similar efficiencies at actin nucleation with 200–400 nM Tmod1 or Tmod3 increasing the concentration of barbed ends up to 3–4-fold when compared with polymerization of actin alone. As expected, Tmod4 had no effect on the concentration of barbed ends.

Because Tmods cap the pointed ends of actin filaments, we predicted that in these experiments, actin assembles from the free barbed ends of actin nuclei stabilized by Tmods. To test this prediction, we measured the kinetics of 0.6 μM actin polymerization in the presence of Tmod3 or the barbed end-binding drug cytochalasin D. Because the critical concentration at the pointed end is 0.6 μM, actin assembles from barbed ends only at this concentration (1). In the control experiment with actin alone, actin assembled slowly (Fig. 1*C*, *black line*). Addition of 5 nM cytochalasin D effectively inhibited polymerization, confirming that actin assembly predominantly occurred at barbed ends under this condition (Fig. 1*C*, *red line*). On the other hand, addition of 50 nM Tmod3 led to a significant acceleration of polymerization, indicating that Tmod3-induced actin polymerization occurs at the barbed ends (Fig. 1*C*, *blue line*).

All Mammalian Tmods Are Capable of Binding to Monomeric Actin—Binding to monomeric actin is a common property of most actin nucleators (43). We showed previously that human Tmod3 and rat Tmod2 bound G-actin, whereas chicken Tmod1 and Tmod4 did not (31). The N-terminal domain of Tmod3 contains G-actin-binding activity (31), but no known G-actin-binding motifs are found in either Tmod2 or Tmod3 (32). Therefore, we introduced point mutations in the N-terminal half of Tmod3 to identify which residues in Tmod3 are essential for G-actin binding. Using an alignment of Tmod isoform sequences (supplemental Fig. S1), we selected and mutated eight residues that are conserved in mammalian Tmod2 and Tmod3, but different from chicken Tmod1 and Tmod4. We also introduced four mutations (L29G, L73D, L134D, and L138V) that were reported previously to disrupt each of the three functional α-helices in N-terminal half of Tmod3 (supplemental Fig. S1) (29, 30, 44). We tested the ability of Tmod3 mutant proteins to bind G-actin by performing chemical cross-linking assays with the zero-length cross-linker, EDC/sulfo-NHS, followed by SDS-PAGE and Coomassie staining. In control assays, actin and Tmod3 proteins were individually reacted with EDC/sulfo-NHS, and these proteins appeared as single bands (Fig. 2*B*). When actin and wild-type mouse or human Tmod3 were mixed, they formed a complex with apparent molecular mass of 80–160 kDa (Fig. 2*A*), consistent with our previous report (31). Unexpectedly, each of the Tmod3 mutant proteins in which residues unique to Tmod2 and Tmod3 had been targeted could be cross-linked to G-actin, similar to wild-type Tmod3 (Fig. 2*A*). Mutations in the first (L29G) and the third (L134D and L138V) helices in the Tmod3 N-terminal domain also had no effect on cross-linking to G-actin (Fig. 2*A*). However, the mutation of Leu-73 in α-helix2 to aspartic acid significantly decreased the formation of the actin-Tmod3 complex (Fig. 2*A*). This mutation is likely to cause a localized disruption in α-helix2 rather than a general disruption of Tmod3 structure. Previous studies have shown that chicken Tmod1-L71D, which corresponds to mouse Tmod3-L73D, exhibits decreased tropomyosin-dependent actin-capping activity, while retaining binding to tropomyosin via the adjacent α-helix1 and α-helix3, similar to wild-type Tmod1 (30, 45). Moreover, the C-terminal LRR domain is distinct from the N-terminal domain and does not depend on the N-terminal

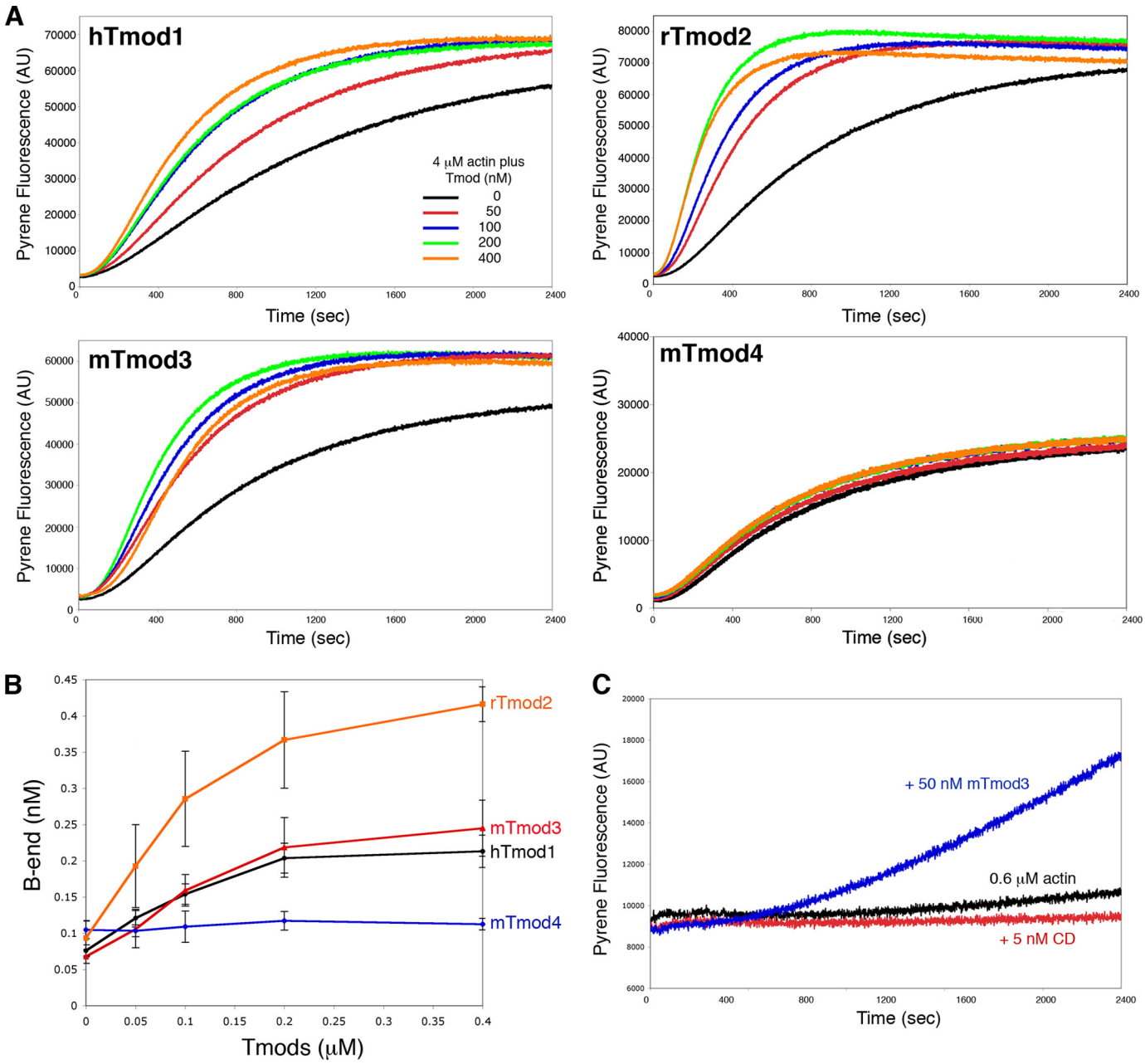

FIGURE 1. **Mammalian Tmod1–3 promote spontaneous actin polymerization, whereas Tmod4 does not.** *A*, human Tmod1 (*hTmod1*), rat Tmod2 (*rTmod2*), mouse Tmod3 (*mTmod3*) or mouse Tmod4 (*mTmod4*) were mixed with 4 μM G-actin (8% pyrenyl), and salts were added to initiate polymerization. Kinetics of actin polymerization were monitored by increased pyrenyl-actin fluorescence, as described under "Experimental Procedures." *B*, concentration of barbed ends as a function of increasing hTmod1 (*black line*), rTmod2 (*orange line*), mTmod3 (*red line*), or mTmod4 (*blue line*) concentrations. The concentration of barbed ends was calculated from the polymerization rate when 50% of monomers were polymerized, as described under "Experimental Procedures." Data shown are mean ± S.D. of three experiments. *C*, actin assembles from barbed ends in the presence of mTmod3. Actin (0.6 μM; 8% pyrenyl) was assembled in the presence of 5 nM cytochalasin D (*CD*; *red line*) or 50 nM mTmod3 (*blue line*). Actin-only control is shown with the *black line*. *AU*, arbitrary units.

domain for folding (20, 46–48). Because Leu-73 in α-helix2 is conserved among all chicken and mammalian Tmod isoforms (supplemental Fig. S1), G-actin binding may be a common property of all Tmod isoforms.

To verify the G-actin-binding ability of Tmod isoforms, we examined the interaction of Tmods with G-actin using nondenaturing PAGE as described by Safer (41). In our previous study, G-actin-binding ability was compared among chicken Tmod1, rat Tmod2, human Tmod3, and chicken Tmod4 using a steady state pyrene assay for critical concentration (Table 1) (31). In this study, in addition to these Tmod isoforms, mouse Tmod3 and mouse Tmod4 were also tested. Because the amino acid sequence of human Tmod1 is 97% identical to mouse Tmod1, and the amino acid sequence of rat Tmod2 is 99% identical to mouse Tmod2, human Tmod1 and rat Tmod2 are considered to be equivalent to mouse Tmod1 and mouse Tmod2. When G-actin and each Tmod were mixed, the actin band became fainter or disappeared entirely as increasing concentrations of Tmods were added (Fig. 3*A*). On the other hand, when G-actin was mixed with Tmod2, a new band indicative of a complex was detected (Fig. 3*A*). The disappearance of the actin band is likely due to a shift up to form a slower mobility Tmod-

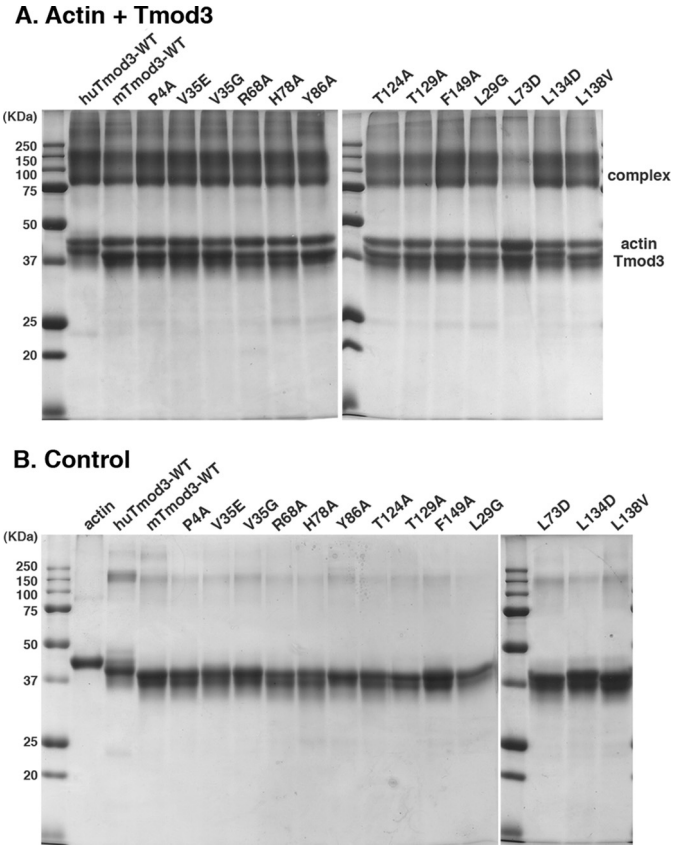

FIGURE 2. **α-Helix disrupting mutation L73D in α-helix2 eliminates Tmod3 cross-linking to G-actin, whereas mutations in the other N-terminal domains of Tmods do not.** *A,* G-actin (8 μM) was mixed with wild-type human Tmod3 (*huTmod3-WT*), wild-type mouse Tmod3 (*mTmod3-WT*), or mutant mTmod3 proteins at an equal molar ratio and incubated at room temperature with EDC/sulfo-NHS for 20 min. The samples were analyzed by SDS-PAGE on 12% acrylamide gels and stained with Coomassie Blue. *B,* control. Actin and Tmod3 proteins were incubated separately with EDC/sulfo-NHS and subjected to electrophoresis as in *A*.

G-actin complex, whereas the Tmod-G-actin complexes (with the exception of the G-actin-Tmod2 complex) appeared to migrate at the same mobility as Tmods alone (Fig. 3*A*). Thus, we could not resolve the Tmod-actin complex from that of the Tmod1, Tmod3, or Tmod4 alone. All Tmods that we tested bound to G-actin, suggesting that G-actin-binding activity is conserved among vertebrate Tmod isoforms. However, not all Tmods were the same. Densitometric analysis of the free (unshifted) G-actin bands showed that both human and mouse Tmod3 exhibited the strongest G-actin-binding activity, in that 50% of 4 μM actin formed a complex at Tmod3 concentrations $\sim$2 μM, whereas the other Tmod isoforms, Tmod1, Tmod2, and Tmod4, bound G-actin with lower efficiencies, in that 50% of 4 μM actin formed a complex at Tmod concentrations greater than 3.5 μM (Fig. 3*B*). These results disagree with our previous report that G-actin binding is a unique characteristic of Tmod3 (31). It is most likely that the higher affinity of Tmod3 for binding to G-actin led to the misinterpretation of data in our previous study.

Tmod3 Forms a 1:1 Complex with G-actin—To determine the stoichiometry of the Tmod3-G-actin complex, we analyzed the complex by gel filtration chromatography using a Superdex 200HR column equilibrated with a low ionic strength buffer (see "Experimental Procedures"). The molecular weight of Tmod3 (39,600 Da) is close to that of G-actin (42,000 Da), and their elution profiles are similar when chromatographed individually (Fig. 4*A*, *red, blue,* and *brown lines*, respectively). Note that the UV absorption of G-actin at 280 nm is much greater than equimolar amounts of Tmod3. When Tmod3 was mixed with G-actin in a 1:1 molar ratio, the elution profile revealed that the peak was shifted toward earlier fractions as compared with each individual protein (Fig. 4*A*, *green line*). SDS-PAGE analysis of the eluted fractions showed that the peak fraction contained both Tmod3 and G-actin (Fig. 4*B*, *panel d*). Densitometric analysis showed that the ratio of band intensities of actin/Tmod3 was 1:0.91 in the peak fraction (Fig. 4*B*, *panel d*), suggesting that Tmod3 and G-actin form a complex with a 1:1 molar ratio. When Tmod3 was mixed with a 2-fold excess amount of G-actin, the elution profile had two major peaks (Fig. 4*A*, *purple line*). The position of the earlier eluting peak in this mixture corresponded to that of the peak in the 1:1 mixture of Tmod3 and G-actin, whereas the later eluting peak corresponded to the free G-actin and Tmod3 peaks (Fig. 4*A*). Using SDS-PAGE, we found that the earlier eluting peak fraction contained both Tmod3 and actin, with a ratio of actin/Tmod3 of 1:1.13 (Fig. 4*B*, *panel e*). On the other hand, the later eluting peak contained the excess G-actin, corresponding to the peak of G-actin alone and contained only the actin band (Fig. 4*B*, *panel e*). These results show that Tmod3 binds to G-actin in a 1:1 molar ratio, because these proteins co-eluted in the earlier peak, whereas excess G-actin eluted in the later peak.

To test whether the inability of the Tmod3-L73D mutant to be chemically cross-linked to actin (Fig. 2) was due to impaired G-actin binding, we investigated the binding of this mutant to G-actin by gel filtration. Addition of an equal concentration of Tmod3-L73D to actin did not change the elution profile of G-actin alone (Fig. 4*A*, *orange line*). This result indicates that the binding affinity of Tmod3-L73D to G-actin has been greatly reduced, which agrees with the results of our cross-linking assay (Fig. 2*A*). Thus, we conclude that Leu-73 is critical for Tmod3 binding to G-actin.

Tmod3 Requires Both N- and C-terminal Domains for Its Nucleating Activity—To determine which domain(s) of Tmod3 are responsible for its actin-nucleating activity, we characterized the effects of recombinant Tmod3 fragments on actin nucleation and G-actin binding. A schematic of these fragments is shown in Fig. 5*A*, where the domain structure of Tmod3 is based on data from experiments on Tmod1. Fragments 1–92 and 43–189 contain the second α-helix (α-helix2) that includes Leu-73. Fragment 150–352 contains the conserved LRR domain, and fragment 1–325 lacks 27 C-terminal residues that have been reported to be critical for the pointed end-capping activity of the C-terminal domain of Tmod1 (20). As described previously, the C-terminal LRR domain does not depend on the N-terminal domain for folding (20, 46–48), indicating that the Tmod3 fragment 150–352 maintains the folded structure of the C-terminal domain. On the other hand, it has been demonstrated that the chicken Tmod1 fragments 1–92 and 109–144 bind to tropomyosin (30, 45), and the chicken Tmod1 fragment 1–92 caps the pointed ends of tropomyosin-coated actin fragments (45). Thus, the fragments 1–92,

TABLE 1

Summary of recombinant Tmods used in this study and their activities

Shown are molecular weights, pI values, extinction coefficients, nucleating activity, G-actin binding activity, and actin filament pointed end capping activity. The abbreviations used are as follows: +, yes; −, no; weak, weakened activity; n.d., not determined.

Tmod	M_r[a]	pI	$Abs_{0.1\%}^{280}$	Nucleating activity	G-actin binding activity				P-end capping Activity (K_d for capping P-end)
					Cross-linking	Nondenaturing-PAGE	Gel-filtration assay	Steady state pyrene assay for critical concentration	
Tmod1 (human)	41,367	5.03	0.532	+	n.d.	+	n.d.	n.d.	+ (0.18 μM) [g]
Tmod1 (chicken)	41,542	4.96	0.353	weak[b]	-[c]	+	n.d.	-[c]	+ (0.11 μM) [d]
Tmod2 (rat)	40,388	5.34	0.148	+	n.d.	+	n.d.	weak[c]	n.d.
Tmod3 (mouse)	39,647	5.02	0.191	+	+	++	+	n.d.	+ (0.18 μM)
Tmod3 (human)	40,492	5.08	0.187	+[c]	+[c]	++	n.d.	+[c]	+ (0.17 μM) [c, e]
Tmod4 (mouse)	40,158	4.76	0.517	-	n.d.	+	n.d.	n.d.	n.d.
Tmod4 (chicken)	39,054	4.91	0.312	n.d.	n.d.	+	n.d.	-[c]	+ (0.08 μM) [f]
Tmod3 fragment and mutant									
1-92	10,719	4.54	0.512	-	n.d.	-	n.d.	n.d.	n.d.
43-189	16,417	4.72	0.280	-	+	++	n.d.	n.d.	-
150-352	23,024	7.05	0.065	-	n.d.	-	n.d.	n.d.	n.d.
1-325	36,577	4.76	0.207	-	n.d.	++	n.d.	n.d.	n.d.
L73D	39,649	4.97	0.191	-	-	-	-	n.d.	n.d.
L134D	39,649	4.97	0.191	+	+	++	n.d.	n.d.	+
L138V	39,633	5.02	0.191	+	+	++	n.d.	n.d.	n.d.
K317A	39,590	4.97	0.191	weak	n.d.	++	n.d.	n.d.	weak
K344A	39,590	4.97	0.191	weak	n.d.	++	n.d.	n.d.	weak
RR345/346AA	39,477	4.92	0.192	-	n.d.	++	n.d.	n.d.	weak

[a] Molecular weights for purified recombinant proteins are shown, including vector- derived sequence.
[b] Data are from Fowler *et al.* (20).
[c] Data are from Fischer *et al.* (31).
[d] Data are from Weber *et al.* (19).
[e] Data are from Fischer *et al.* (27).
[f] Data are from Weber *et al.* (66) and Almenar-Queralt *et al.* (18).
[g] V. M. Fowler, unpublished data.

43–189, and 1–325 we tested were predicted to maintain the functional structure of the α-helices. Each of the purified recombinant Tmod3 fragments had the expected molecular weights, based on separation using SDS-PAGE (Table 1 and Fig. 5*B*).

First, we tested the ability of Tmod3 fragments to bind G-actin using nondenaturing PAGE. As shown above in Fig. 3, full-length Tmod3 formed a complex with G-actin, as evident by the gradual disappearance of the actin band as the concentration of full-length Tmod3 increased (Fig. 5*C*, *red dot*). Although fragment 1–92 contains Leu-73, the intensity of the actin band was not diminished, indicating that 1–92 did not form a complex with G-actin (Fig. 5*C*, *red dot*). On the other hand, when G-actin was mixed with fragment 43–189, which also contains Leu-73, the intensity of the actin band decreased (Fig. 5*C*, *red dot*), and a third band, which represents the complex, appeared (Fig. 5*C*, *green dot*). Fragment 1–325, which completely encompasses residues 43–189, also formed a complex with G-actin similar to fragment 43–189 (Fig. 5*C*). On the other hand, the C-terminal fragment 150–352 did not form a complex with actin, as the intensity of the actin remained unchanged in the presence of increasing amounts of 150–352 (Fig. 5*C*, *red dot*). These results indicate that residues 43–189 of Tmod3, which includes α-helix2, are sufficient for binding G-actin.

Next, to investigate the relationship of monomer binding to nucleation, we tested the ability of these Tmod3 fragments to nucleate actin polymerization in a pyrene-actin polymerization assay. Although full-length Tmod3 enhanced actin polymerization as shown in Fig. 1*A*, none of the Tmod3 fragments enhanced actin polymerization, including 1–325 or 43–189 which can bind monomers (Fig. 5*D*). Taken together, these results demonstrate the following: 1) both the N- and C-terminal domains are necessary for actin nucleation by Tmod3; 2) the G-actin-binding region of Tmod3 (residues 43–189) is not sufficient for actin nucleation, and 3) the 27 residues at the C terminus of Tmod3 (residues 326–352) are necessary for actin nucleation.

Tmod3 Binds to G-actin over an Extended Interface—To identify interaction sites on G-actin and Tmod3, we performed chemical cross-linking with EDC/sulfo-NHS followed by mass

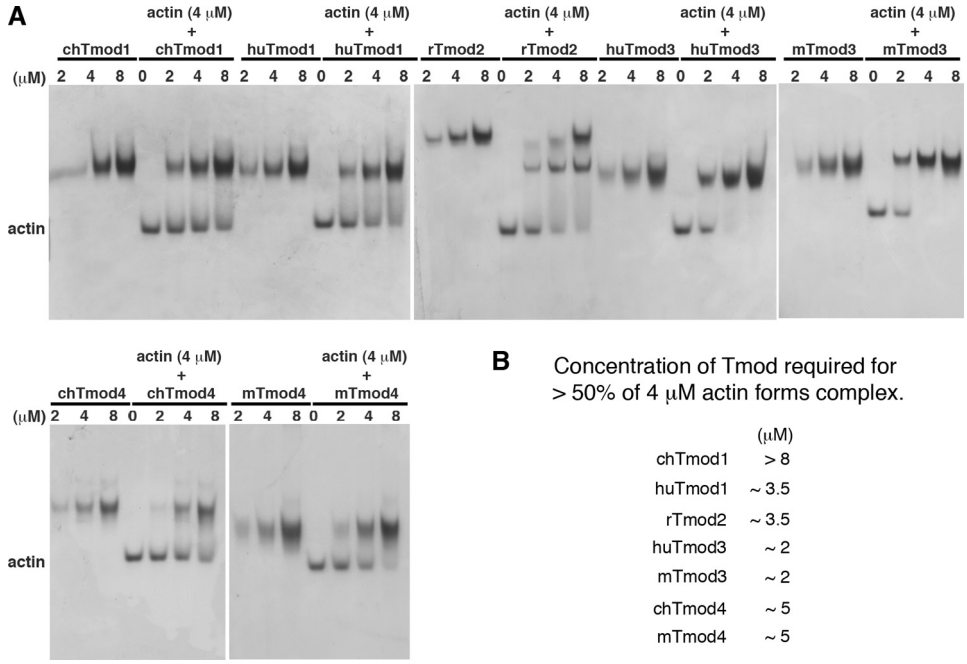

FIGURE 3. **Vertebrate Tmod isoforms bind to G-actin with different efficiencies.** *A,* interaction between G-actin and various Tmod isoforms was examined by nondenaturing PAGE. Tmod alone (2, 4, and 8 μM), and 4 μM G-actin with Tmod (0, 2, 4, and 8 μM) were incubated for 20 min at room temperature, and samples were analyzed by nondenaturing PAGE on 10% acrylamide gels. In the presence of both proteins, the band of actin became less intense as the concentration of Tmod increased, indicating formation of a complex. *B,* concentration of each Tmod isoform required for more than 50% of 4 μM actin to form a complex was determined by a densitometric analysis of the actin bands and is indicated.

spectrometry to identify the resulting cross-linked peptides (49). Full-length Tmod3 or the Tmod3 fragment 43–189 and G-actin were incubated with EDC/sulfo-NHS, and then the resulting reaction products were separated by BisTris NuPAGE (see "Experimental Procedures"). Two slower migrating cross-linked bands with apparent molecular masses of 75–100 kDa were observed only when full-length of Tmod3 and G-actin were mixed with EDC/sulfo-NHS, consistent with Fig. 2 and our previous report (Fig. 6*A*) (31). Similarly, Tmod3 fragment 43–189 formed a complex with G-actin also displaying two bands, but with apparent molecular masses of ~60 kDa (Fig. 6*A*). We performed in-gel trypsin digestion for each cross-linked band and matching uncross-linked protein followed by nanocapillary HPLC-tandem mass spectrometry (LC-MS/MS). Detailed analysis of LC-MS/MS datasets to identify inter-chain cross-links were initially focused on the Tmod-(43–189)-actin complex. When high confidence cross-links were identified in this sample, the full-length Tmod/actin dataset was evaluated to confirm that the same cross-link occurred in this larger protein complex. The full-length Tmod/actin data were not independently searched for cross-links unique to this larger complex due to the far greater complexity of the full-length Tmod/actin LC-MS/MS datasets and the difficulty in identifying cross-linked peptide spectra with existing software tools.

These analyses identified six sets of Tmod-actin cross-linked peptides that involved five regions of Tmod and three regions of actin (Table 2). In two of the cross-linked complexes, the Tmod3 cross-linked sites (Glu-74 and Glu-79) are located in or near Tmod3 α-helix2 (residues 67–77), supporting our data from characterization of the Tmod3-L73D mutant that indicate the importance of α-helix2 in binding to G-actin. Both Glu-74 and Glu-79 were cross-linked to Lys-61 (Fig. 6*B*, supplemental Figs. S2 and S3, and supplemental Tables 2 and 3), in actin subdomain 2, which is the exposed domain on pointed ends of actin filaments (Fig. 6*B*). Interestingly, four different Tmod3 lysine residues (Lys-54, Lys-94, Lys-96, and Lys-169) were cross-linked to either Asp-24 or Asp-25 in subdomain 1 (Table 2 and Fig. 6*B*). Although there is no known structure for the N-terminal region of Tmod3, these data indicate that these lysine residues are in close proximity in the folded protein because EDC/sulfo-NHS cross-links will only form between residues that are within salt bridge distances. Finally, Tmod3 Lys-94 is also cross-linked to either actin Glu-99 or Glu-100. Evaluation of the actin crystal structure shows that the side chains of actin Asp-24 and Glu-100 are ~15 Å apart (Fig. 6*C*). Because lysine and acidic side chains are highly flexible, it is feasible for residues that are up to 10 Å apart to form cross-links when EDC/sulfo-NHS is used. Therefore, it is possible for both indicated actin sites to form independent cross-links with Tmod3 Lys-94, if the Tmod3 Lys-94 is positioned between these two acidic actin residues as schematically illustrated in Fig. 6*C*. Because Tmod3-(43–189) forms cross-links with sites in actin subdomains 1 and 2 (Fig. 6*B*), it is apparent that the G-actin-binding region of Tmod3 interacts with G-actin over an extended interface.

Both the G-actin-binding and Pointed End-capping Activities of Tmod3 Are Necessary for Actin Nucleation—To determine more precisely which region of Tmod3 is necessary for actin nucleation, we examined the effect of Tmod3 mutant proteins on pyrene-actin polymerization. The schematic in Fig. 5*A* shows the locations of the Tmod3 residues that we mutagenized. In addition to the Tmod3-L73D mutant, which exhibits decreased G-actin-binding activity (Figs. 2 and 4), we selected two other mutants (L134D and L138V) whose mutations are located in α-helix3 located in the G-actin-binding region (residues 43–189). Both Tmod3-L134D and Tmod3-L138V cross-link to G-actin in a cross-linking assay (Fig. 2), and the L134D and L138V mutations disrupt α-helix3 in Tmod1, thereby abolishing tropomyosin-binding activity (29, 44). We also introduced one or two point mutations in four C-terminal Tmod3 residues (K317A, K344A, and R345A/R346A) that are highly conserved among Tmod isoforms (Figs. 5*A* and 9*B*) and located on the molecular surface based on the crystal structure of the C-terminal half of chicken Tmod1 (50).

Tmod3-L134D and L138V nucleated actin polymerization, creating new free barbed ends in a similar manner as wild-type

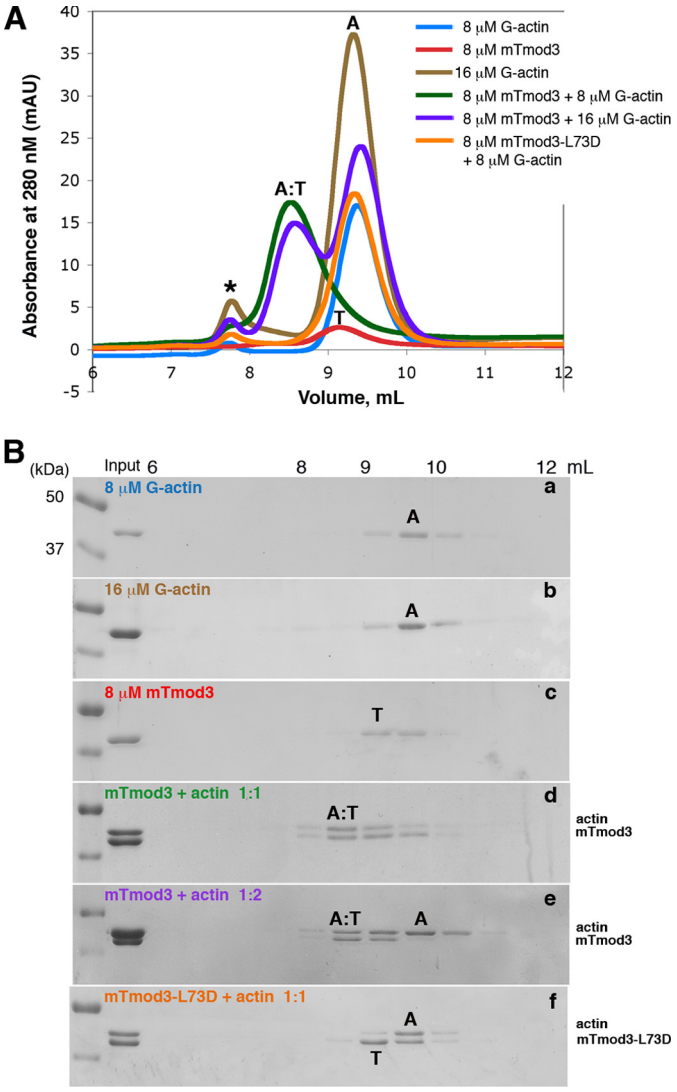

FIGURE 4. **G-actin and Tmod3 form a 1:1 complex in gel filtration chromatography.** Indicated concentrations of G-actin, Tmod3, or a mixture of G-actin and Tmod3 were loaded on a Superdex 200HR column and eluted in a low ionic strength buffer. *A,* elution profiles. *B,* SDS-PAGE analysis of eluted fractions. The fractions marked "*A:T*" correspond to a Tmod3-actin complex that elutes as the first major peak from the column. The peaks of unbound G-actin (*A*) and Tmod3 (*T*) were also indicated. The *asterisk* in the elution profile indicates a small peak at the void volume present in the actin samples that may represent low amounts of seeds in the actin preparations. *mAU*, milli-absorbance units.

Tmod3, indicating that α-helix3 of Tmod3 is not necessary for its actin-nucleating activity (Fig. 7, *A*, *C*, and *D*). On the other hand, the other four mutant proteins (L73D, K317A, K344A, and R345A/R346A) exhibited significantly decreased actin-nucleating activity (Fig. 7, *B* and *E–G*). Tmod3-L73D and R345A/R346A had no detectable effect on actin polymerization, whereas Tmod3-K317A and K344A exhibited weak actin-nucleating activity in a concentration-dependent manner (Fig. 7, *B* and *E–G*). The effects of Tmod3-K317A and K344A on the concentration of new barbed ends were only ~1.3- and ~1.8-fold greater than the actin-only control, respectively, at the highest concentration tested (Fig. 7*H*). This is significantly weaker than wild-type Tmod3, which induced an ~3.2-fold increase in the concentration of barbed ends compared with the actin-only control (Fig. 7*H*).

Next, we examined the interaction of the Tmod3 C-terminal mutants (K317A, K344A, and R345A/R346A) and the N-terminal mutants (L73D, L134D, and L138V) with G-actin using nondenaturing PAGE. As first shown in Figs. 3 and 5, the intensity of the actin band decreased as the concentration of wild-type Tmod3 increased (supplemental Fig. S4). Increasing amounts of Tmod3-L73D did not form a complex with G-actin (supplemental Fig. S4), corroborating our previous results from cross-linking and gel filtration assays (Figs. 2*A* and 4). The other five mutant proteins all formed complexes with G-actin, based on diminution of intensity of the actin band upon increasing concentrations of the mutant Tmods, indicating that these mutant proteins have intact G-actin-binding activity (supplemental Fig. S4). Because Tmod3-L73D was unable to bind G-actin or to nucleate actin assembly, these two activities appear to be related. However, the three C-terminal mutant proteins (K317A, K344A, and R345A/R346A) bind G-actin normally (Fig. 8) but show decreased actin-nucleating activity (Fig. 7). Therefore, in contrast to α-helix2 containing Leu-73, the C-terminal residues of Tmod3 contribute to actin nucleation without contributing to G-actin binding.

Our previous study showed that 38 residues at the C terminus of chicken Tmod1 were critical for actin pointed end-capping in the absence of tropomyosin (20). Based on these results, we sought to determine whether or not the pointed end-capping activity of Tmod3 is linked to its actin-nucleating activity. To address this, we tested the pointed end-capping ability of wild-type and mutant Tmod3 proteins by measuring actin elongation rates from gelsolin-capped actin seeds (19, 20). Wild-type Tmod3 inhibited elongation from the pointed ends of gelsolin-capped actin filaments in a concentration-dependent manner, as expected, with ½ maximum inhibition at ~0.18 μM (Fig. 8, *closed circle*). On the other hand, all three C-terminal mutants (K317A, K344A, and R345A/R346A) were less effective at inhibiting actin polymerization from pointed ends (Fig. 8, *open circle*, *triangle*, and *square*, respectively). The extent of pointed end-capping by wild-type Tmod3 plotted in Fig. 8 appeared to have an exponential dependence on Tmod concentration, whereas the plots for the Tmod3 C-terminal mutants appeared to have a relatively linear dependence on Tmod concentration. One possible explanation is that G-actin sequestration by Tmod3 may contribute to inhibition of actin elongation in these assays, accounting for the apparent pointed end-capping activity of Tmod3 C-terminal mutants that can still bind actin monomers (supplemental Fig. S4).

To address this possibility, we estimated the concentration of the G-actin-Tmod3 complex in each assay by using the K_d value of human Tmod3 for G-actin binding (~0.51 μM) that was determined previously from Tmod3 inhibition of G-actin binding to thymosin-β4 (31). We subtracted the concentration of the G-actin-Tmod3 complex from the total G-actin concentration, and we then calculated a theoretical polymerization rate assuming that Tmod3 possesses only G-actin-binding and -sequestering activity but does not cap pointed ends (also see "Experimental Procedures") (Fig. 8, *closed diamond* with *dashed line*). The theoretical rate was close to the rate measured in the presence of the Tmod3-(43–189) fragment (Fig. 8, *closed triangle* with *dashed line*), which is a minimal fragment that

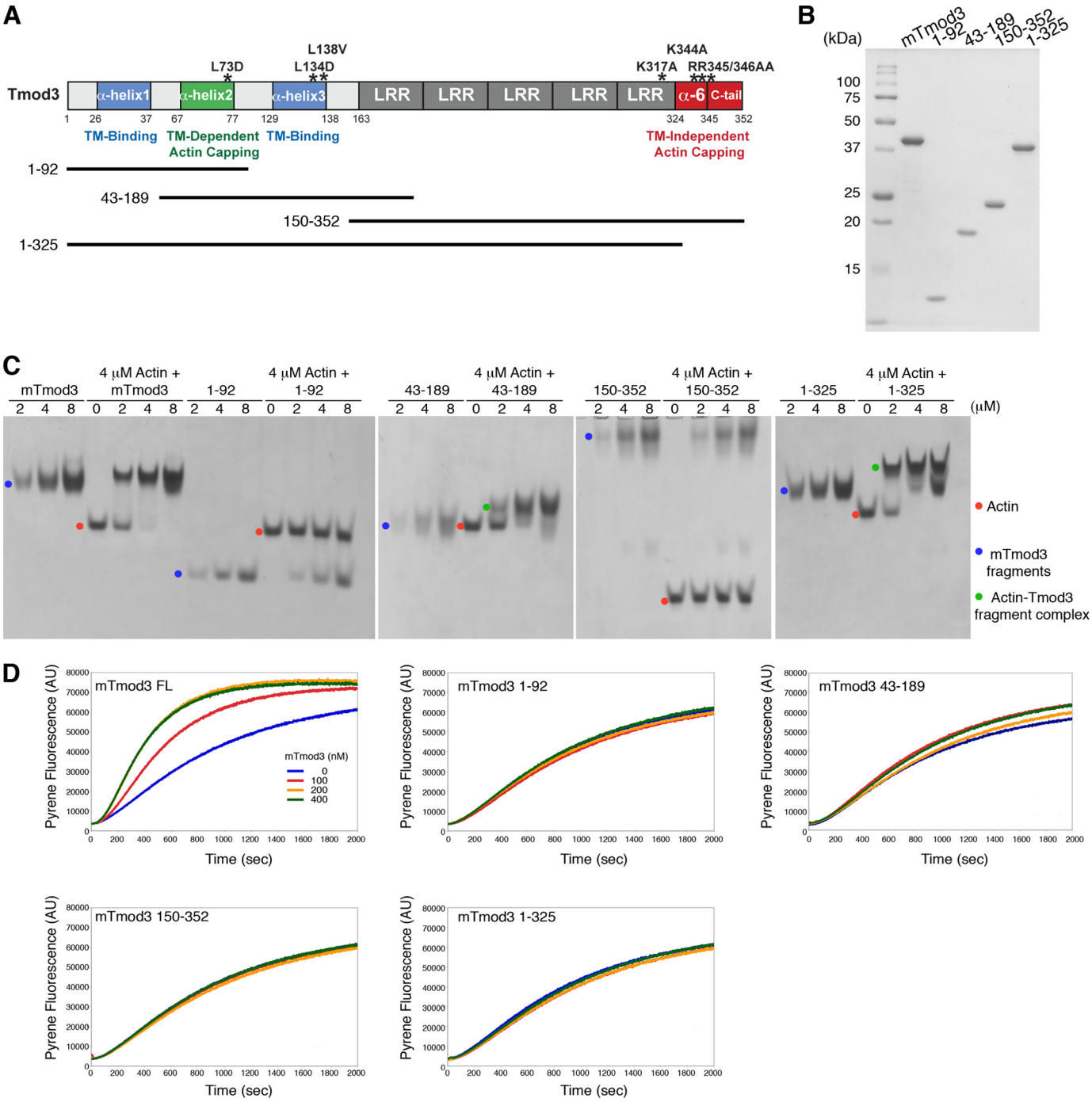

FIGURE 5. **Tmod3 fragments containing residues 43–189 bind to G-actin but do not promote actin polymerization.** *A,* schematic diagram of structural domains of Tmod3 based on data from Tmod1, locations of Tmod3 fragments, and sites of mutations for proteins analyzed in Figs. 7–9. *B,* Coomassie Blue-stained gel of recombinant Tmod3 fragments. 0.5-μg amounts of each fragment were electrophoresed on a 12% SDS-polyacrylamide gel. *C,* nondenaturing PAGE analysis of G-actin binding to full-length Tmod3 or Tmod3 fragments at indicated concentrations, as in Fig. 3. *Red dots,* actin. *Blue dots,* Tmod3 fragment. *Green dots,* G-actin-Tmod3 fragment complex. *D,* effects of Tmod3 fragments on spontaneous actin polymerization, as in Fig. 1. *AU,* arbitrary units.

bound G-actin but did not nucleate actin assembly, suggesting that the theoretical values were accurate. The polymerization rate in the presence of each Tmod3 C-terminal mutant was less than predicted for a Tmod3 that can only sequester monomers, thus indicating that the Tmod3 C-terminal mutants still possess some residual pointed end-capping activity. Importantly, Tmod3 R344A exhibited the strongest pointed end capping (Fig. 8, *opened triangle*) and actin nucleating (Fig. 7) activities of the three C-terminal mutants, providing further evidence that these two activities of Tmod3 are correlated.

DISCUSSION

In this study, we demonstrate that mammalian Tmod1–3 all nucleate actin assembly, creating free barbed ends. Our data characterizing truncated fragments and point mutations of Tmod3 suggest that two distinct actin-binding activities of

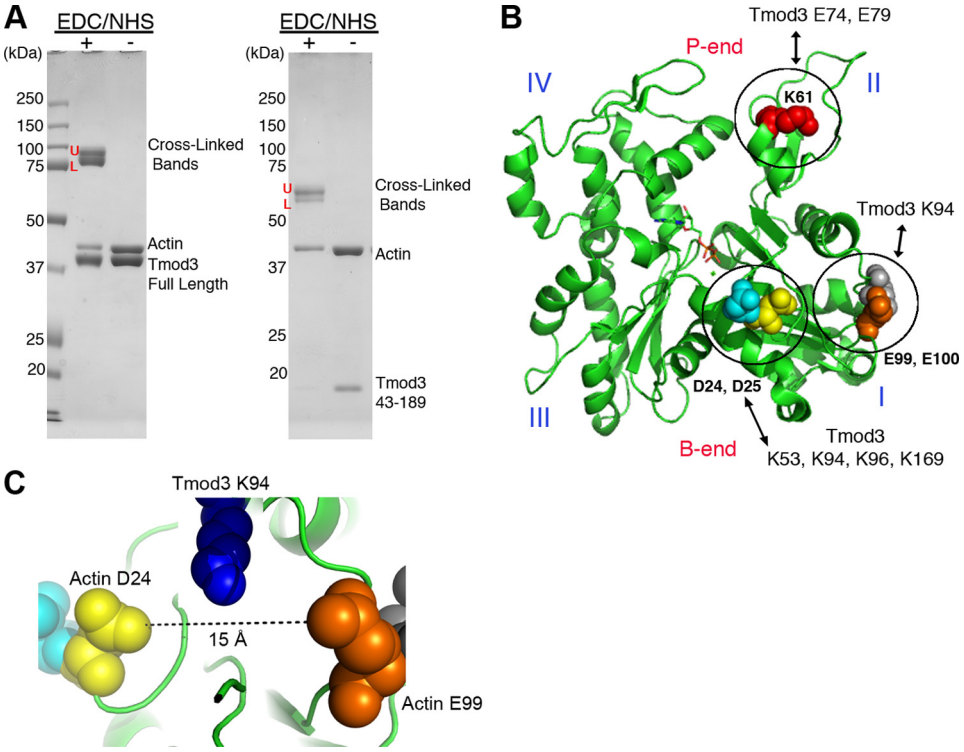

FIGURE 6. **Sequence identification of chemically cross-linked peptides between Tmod3 and G-actin indicates the N-terminal domain of Tmod3 interacts with actin subdomains 1 and 2.** *A,* full-length Tmod3 (*left*) or Tmod3 fragment 43–189 (*right*) was incubated with G-actin in the presence or absence of EDC/sulfo-NHS. The resulting samples were analyzed by 10% BisTris NuPAGE. Each upper band (*U*) and lower band (*L*) of cross-linked bands was analyzed by a combination of in-gel trypsin digestion and LC-MS/MS. *B,* Schutt actin model (Protein Data Bank code 2BTF (67)), with the position of lysine residue (*K61* in *red*) cross-linked with Tmod3-(69–75)- or -(76–81)-peptide, aspartic acids (*D24* in *yellow* and *D25* in *cyan*) cross-linked with Tmod3-(52–58)-, -(94–96)-, -(94–101)-, -(95–101)-, or -(164–172)-peptide, and glutamic acids (*E99* in *orange* and *E100* in *gray*) cross-linked with Tmod3-(94–96)-peptide are shown. Actin subdomains (*I–IV*) are also indicated. *C,* distance between actin residues Asp-24 (*yellow*) and Glu-99 (*orange*) is about 15 Å. A Tmod residue Lys-94 (*blue*) located between these two residues as illustrated would be within cross-linking distance of both sites as observed in the current cross-linking experiments.

Tmod3 support its actin-nucleating activity. The first is G-actin-binding activity, which is present in the mostly unstructured N-terminal domain utilizing residues between 43 and 189 in Tmod3, and the other is actin filament pointed end-capping activity, conferred by residues in the β-sheet of fifth LRR and α6-helix in the folded C-terminal domain.

Seven types of actin-nucleating proteins have been described as follows: Arp2/3 (7), formins (51), spire (10), cordon-bleu (8), Lmod2 (11), JMY (9), and vinculin (15). Compared with most of these other actin-nucleating proteins, the actin-nucleating activity of Tmod1–3, which increases the rate of polymerization up to 3–5-fold, is relatively weak. The activated Arp2/3 complex is the strongest of these actin nucleators as it enhances the nucleation rate up to several thousandfold at nanomolar concentrations (52). Spire, cordon-bleu, and JMY exhibit similar degrees of actin-nucleating activity, increasing the nucleation rate ~10-fold at nanomolar concentrations (8–10). Fifteen formin proteins identified in mammals exhibit a wide range of actin-nucleating activities with most formin proteins showing stronger activity than Tmod1–3 (51). However, because formins promote both nucleation and elongation processes during actin assembly (53), it is difficult to compare their activity directly to Tmods using the data that we collected using bulk pyrenyl-actin polymerization assays. The effect of vinculin on the rate of nucleation has not yet been demonstrated (15).

The retention of a lag phase of polymerization in the presence of Tmod1–3 suggests that Tmod1–3 accelerate actin assembly but do not bypass nuclei formation (Fig. 1). Indeed, Tmod3 forms a 1:1 complex with G-actin (Fig. 4), which is different from the stoichiometry of spire, cordon-bleu, and JMY that bind multiple G-actins via their tandem WH2 domains, thereby bypassing the nucleation process starting from G-actin (8–10). Therefore, we hypothesize that Tmods promote actin assembly by stabilizing spontaneously forming actin nuclei in a similar manner to actin assembly induced by CapZ, an actin filament barbed end-capping protein (54, 55). CapZ, which caps barbed ends of actin filaments, but does not have G-actin-binding activity, promotes actin assembly with nanomolar concentrations (54, 55). However, importantly, Tmods are also different from CapZ in that actin assembles from free barbed ends in the presence of Tmods (Fig. 1*C*), whereas CapZ stabilizes actin nuclei which polymerize from pointed ends (56).

Tmods share their domain organization with Lmod2, which contains a Tmod-like unstructured N-terminal domain followed by a Tmod-like C-terminal LRR domain in the first ~340 residues of Lmod2 that are ~40% identical and ~60% similar to Tmods (11, 14). Lmod2 further contains a C-terminal extension with ~150 amino acids that include a polyproline region, two predicted helical structures, and a WH2 domain (11, 14). Due to the presence of this WH2 domain in its C-terminal extension, Lmod2 shows much stronger actin-nucleating activity than Tmods, and it increases the nucleation rate up to several thousandfold at nanomolar concentrations, similar to the activated Arp2/3 complex (11, 52). However, the Lmod2 fragment 1–342 containing the Tmod-related domains increases the nucleation rate only ~9-fold (11), which is relatively similar to the actin-nucleating activities of Tmod1–3. Thus, Tmod1–3 and the Tmod-related domains of Lmod2 might nucleate actin assembly in a similar manner. Future studies to characterize the G and F-actin-binding sites and affinities of the Tmod-like regions of Lmod2 will be required to investigate this question.

Actin Monomer Binding by Tmod—Characterization of the Tmod3 L73D mutant revealed that the predicted α-helix2 (residues 67–77) in the G-actin-binding region (residues 43–189) of Tmod3 is necessary for both the G-actin binding and actin-

TABLE 2
Identification of peptide cross-links between Tmod3 and G-actin

Tmod Construct	Gel Band	Observed MH+	z[b]	Mass Error (ppm)	Cross-linked Peptides[a]	
					Tmod	Actin
43-189	Upper	2201.11475	3	2.9	LLSYL**E**K (74)	DSYVGDEAQS**K**R (61)
43-189	Lower	2201.11499	3	3.0	LLSYL**E**K (74)	DSYVGDEAQS**K**R (61)
43-189	Lower	2201.11133	4	1.3	LLSYL**E**K (74)	DSYVGDEAQS**K**R (61)
Full Length	Lower	2201.11060	4	1.0	LLSYL**E**K (74)	DSYVGDEAQS**K**R (61)
43-189	Lower	2061.00220	3	1.3	QAL**E**HK (79)	DSYVGDEAQS**K**R (61)
43-189	Upper	2061.00098	3	0.7	QAL**E**HK (79)	DSYVGDEAQS**K**R (61)
Full Length	Lower	2061.00391	3	2.1	QAL**E**HK (79)	DSYVGDEAQS**K**R (61)
43-189	Upper	1289.65955	3	0.1	**K**GK (94)	AGFAG**DD**APR (24/25
43-189	Upper	1888.04248	3	0.7	KG**K**IFIPK (96)	AGFAG**DD**APR (24/25
43-189	Lower	1759.94897	4	0.1	G**K**IFIPK (96)	AGFAG**DD**APR (24/25
Full Length	Lower	1289.65930	3	0.3	**K**GK (94)	AGFAG**DD**APR (24/25
Full Length	Lower	1888.04382	4	0.3	KG**K**IFIPK (96)	AGFAG**DD**APR (24/25
43-189	Upper	1790.87781	4	0.1	Q**K**NQTSK (53)	AGFAG**DD**APR (24/25)
43-189	Lower	1790.88013	3	1.2	Q**K**NQTSK (53)	AGFAG**DD**APR (24/25)
Full Length	Lower	Accurate Mass Precursor Ion confirmed[c]				
43-189	Upper	1975.00403	4	0.5	FPNVV**K**GEK (169)	AGFAGD**D**APR (25)
43-189	Upper	1975.00659	3	1.7	FPNVV**K**GEK (169)	AGFAGD**D**APR (25)
43-189	Lower	1975.00403	4	0.5	FPNVV**K**GEK (169)	AGFAGD**D**APR (25)
43-189	Lower	1975.00671	3	1.8	FPNVV**K**GEK (169)	AGFAGD**D**APR (25)
Full Length	Lower	1975.00708	3	2.0	FPNVV**K**GEK (169)	AGFAGD**D**APR (25)
Full Length	Lower	1975.00305	4	0.1	FPNVV**K**GEK (169)	AGFAGD**D**APR (25)
43-189	Upper	2269.25879	3	1.7	**K**GK (94)	VAP**EE**HPTLLTEAPLNPK(99/100)
43-189	Lower	2269.25879	3	1.7	**K**GK (94)	VAP**EE**HPTLLTEAPLNPK(99/100)
43-189	Lower	2269.25586	4	0.4	**K**GK (94)	VAP**EE**HPTLLTEAPLNPK(99/100)
43-189	Lower	2269.25488	5	0.1	**K**GK (94)	VAP**EE**HPTLLTEAPLNPK(99/100)
Full Length	Lower	2269.25854	3	1.6	**K**GK (94)	VAP**EE**HPTLLTEAPLNPK(99/100)

[a] Cross-linked residues are highlighted in boldface type, and residue numbers based on full-length protein sequence without extra residues from cloning are shown in parentheses. When MS/MS spectra could not distinguish between adjacent candidate cross-link sites, both sites are highlighted.
[b] z = charge state of precursors in MS scan.
[c] Cross-linked peptide confirmed by the presence of expected precursor ion at correct retention time using an extracted ion chromatogram with a 5 ppm mass error window; no ms/ms spectra were triggered.

nucleating activities of Tmod3. Residues 74 and 79 in Tmod3 α-helix2 and immediately following this helix are in direct contact with G-actin because they were cross-linked to the actin peptide residues 51–62 in subdomain 2, which is the exposed domain on pointed ends of actin filaments. Previous studies suggest that this α-helix2 of Tmod1 is required for high affinity capping of actin filament pointed ends ($K_d \sim 50$ pM) in a tropomyosin-dependent manner (29, 30). These data suggest that α-helix2 of Tmod3 could interact with an identical site located in subdomain 2 of G-actin and at the pointed end of tropomyosin-coated actin filament.

Characterization of the G-actin-binding ability of the Tmod3 fragments also indicated that residues distal to α-helix2 in the N-terminal domain (residues 93–189) are also required for interaction with G-actin, because Tmod3 fragment 1–92 exhibits no G-actin-binding activity (Fig. 5*C*). This is supported by the observation that Tmod Lys-53, Glu-74, Glu-79, Lys-94, Lys-96, and Lys-169 all cross-link to G-actin residues in both subdomains 1 and 2, indicating that the G-actin-binding region of Tmod3 interacts with G-actin over an extended interface (Fig. 6*B* and Table 2). In our previous study, we had identified two potential G-actin-binding sites in human Tmod3 based on tryptic digestion and peptide mapping by LC/MS analysis of an EDC/sulfo-NHS cross-linked G-actin-Tmod3 complex (31). However, the previous study was only able to identify the disappearance of peptides upon cross-linking rather than direct identification of cross-linked products because that study used a less sensitive low mass accuracy mass spectrometer. In contrast, this study exploited the high sensitivity and high mass accuracy of an LTQ Orbitrap mass spectrometer along with improved data analysis strategies and focused on the more informative high confidence identification of cross-linked residues rather than the disappearance of peptides upon cross-linking. In the previous study, the two Tmod peptides that were observed to disappear upon cross-linking were residues 31–40 and 149–169. The first peptide is not present in the mouse

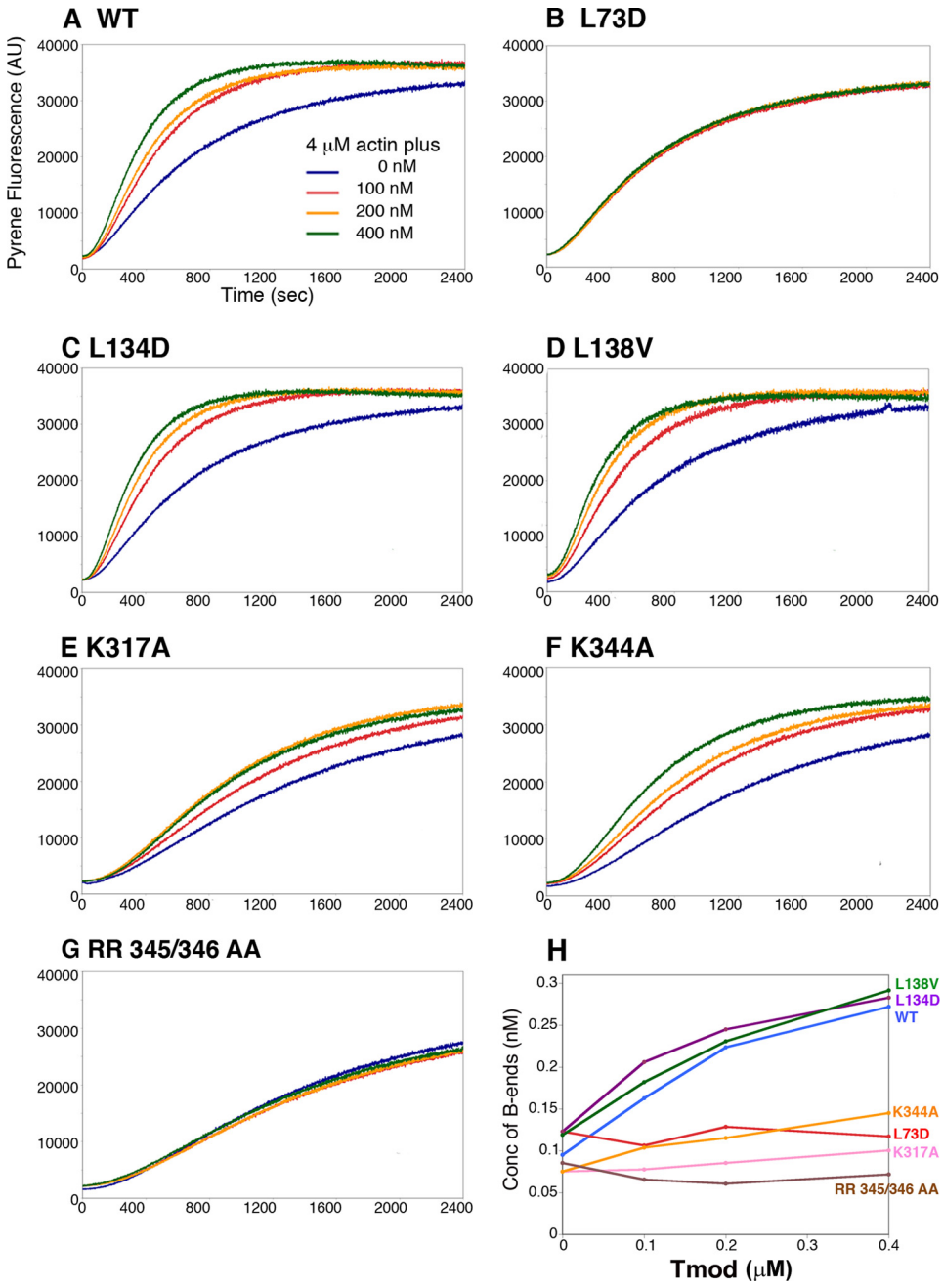

FIGURE 7. **Mutational analysis shows that α-helix2 in the N-terminal domain and the C-terminal tail of Tmod3 are both required to promote actin polymerization.** *A–G,* effect of Tmod3 mutant proteins on spontaneous pyrenyl-actin polymerization was analyzed as in Fig. 1*A*. *H,* concentration of barbed ends as a function of increasing wild-type and mutant Tmod3 concentrations. The concentration of barbed ends was calculated as in Fig. 1*B*. Data shown are means of two independent experiments. *AU*, arbitrary units.

Tmod-(43–189), which was the focus of the current cross-linking analysis. The human Tmod peptide-(149–169) identified in the previous study overlaps the mouse Tmod peptide-(164–172) containing Lys-169, which is shown to be cross-linked to actin Asp-25 in this study and is conserved in both the mouse and human proteins. Therefore, the disappearance of the human-(149–169)-peptide upon cross-linking in the previous study was most likely due to the formation of the Tmod Lys-169-actin Asp-25 cross-link observed in this study.

We could not find any linear sequence similarities either in the G-actin-binding region of Tmod3 or in its entire sequence to most known G-actin-binding motifs, including the WH2, actin-depolymerizing factor-homology or profilin domains, or the actin monomer-binding linker found in JMY and spire (9, 32). However, when we compared the sequence around α-helix2 of Tmod3 with thymosin-β4, we found that a short sequence (Tmod3 residues, ^{74}EKQALE^{79}) present in the Tmod3 peptides cross-linked to actin subdomain 2 exhibited similarity to the C-terminal end of thymosin-β4 (supplemental Fig. S6). Thymosin-β4 is a conserved and abundant actin-sequestering protein with a molecular mass of about 5 kDa (57). Chemical cross-linking, NMR spectroscopy, and crystallographic studies have shown the C-terminal helix of thymosin-β4 interacts with the interface between actin subdomains 2 and 4 (58–60). Although the precise actin residues that interact with thymosin-β4 do not match the actin subdomain 2 peptide cross-linked to α-helix2 of Tmod3, it is attractive to speculate that thymosin-β4 and Tmod3 might share convergent structural features for binding in similar but nonidentical sites of subdomain 2 at the pointed end face of actin molecules. It may be significant that Tmod3 is an effective inhibitor of thymosin-β4 binding to actin monomers (31). Structural analysis of a Tmod3-G-actin complex will be required for further comparison of Tmod3 and thymosin-β4 interactions with G-actin.

Actin Filament Pointed End-capping by Tmod—The C-terminal half (residues 160–344) of chicken Tmod1-(1–359) has been crystallized and is composed of a series of five LRRs, each consisting of an α-helix/β-sheet pair, followed by a sixth α-helix (α6) (50) (Fig. 9*A*). This C-terminal structure is conserved among all Tmods, and following the α6-helix each Tmod isoform has a unique C-terminal tail with a distinct length (Fig. 9*B*). The truncation of the C-terminal α6-helix and/or the C-terminal tail of chicken Tmod1 reduces pointed end-capping activity (20). Based on analysis of the crystal structure, Kreiger *et al.* (50) proposed a docking model for the Tmod1 C-terminal fragment 160–344 at the actin filament pointed end. In this model, the positively charged β-surface of the LRR of Tmod1 interacts with the negatively charged actin helix Ala-181 to Glu-195, placing the tip of

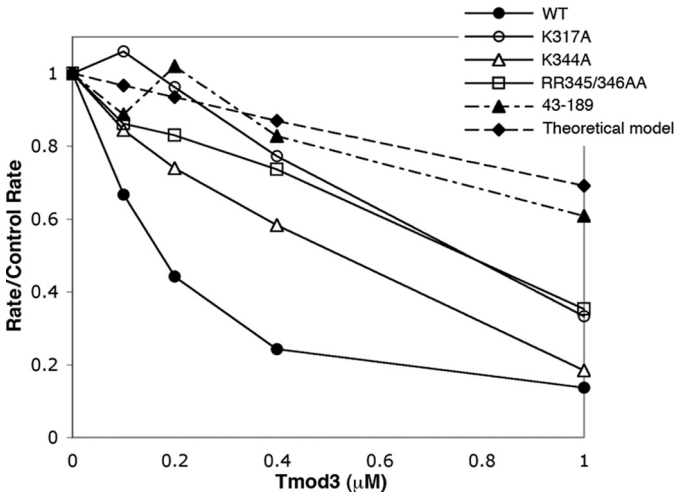

FIGURE 8. **Tmod3 K317A, K344A, and R345A/R346A mutations in the C-terminal domain reduce ability of actin filament pointed end-capping by Tmod3.** Inhibition of pointed end elongation by wild-type Tmod3, Tmod3 mutants, or Tmod3 fragment 43–189 is plotted as the initial rate of elongation in the presence of Tmod3 mutants or the fragment, divided by the initial rate of elongation for actin alone (rate/control rate) as a function of concentration of Tmod3 or fragments. Row data of each assay is shown in supplemental Fig. S5. Wild-type Tmod3 (*closed circle*), Tmod3-K317A (*open circle*), K344A (*open triangle*), R345A/R346A (*open square*), Tmod3 fragment 43–189 (*closed triangle* with *dashed line*), and the theoretical model (*closed diamond* with *dashed line*) assume that Tmod3 possesses only G-actin-binding activity.

the α6-helix at the entrance of the major groove of the actin filament. The cluster of basic residues (RKRR; residues 340–343 in Tmod1, see Fig. 9*B*) at the C-terminal end of the α6-helix is proposed to interact with the highly negatively charged groove on the actin filament, and a hydrophobic region further up this α6-helix is proposed to interact with the hydrophobic "plug" on actin. Our mutational analysis with Tmod3-K344A and R345A/E346A mutants strongly supports this model, because mutations in this cluster of basic residues (RKRR) of the α6-helix of Tmod3 effectively reduce the pointed end-capping activity (Fig. 8). Interestingly, mouse Tmod4 has two glutamine substitutions for these basic residues and a very short C-terminal tail (Fig. 9*B*). Therefore, it is possible that mouse Tmod4 has a weaker affinity for the pointed end of the actin filament compared with the other Tmod isoforms, resulting in a lack of significant actin-nucleating activity. In addition, mutation of Lys-317 in the β-sheet of the fifth LRR (Fig. 8) also reduces the pointed end activity. Although our previous study showed that chicken Tmod1 fragment 1–322 containing the LRRs did not interact with the actin filament pointed end (20), the LRRs may play a role in positioning the α6-helix relative to actin, as proposed in the docking model, but themselves bind to actin with weak affinity. The other possibility is that Lys-317 is critical for folding the α6-helix and/or the C-terminal tail. Additional mutational studies in the LRRs and structural analysis of the Tmod3 mutant proteins are required for further progress in defining the molecular interaction of the C-terminal actin-capping domain of Tmod with the actin filament pointed end.

Actin Nucleation by Tmods—Based on our results and the previous studies on the interaction between Tmods and actin as described above, we propose a mechanistic model of actin nucleation by Tmod1–3 (Fig. 9*C*). First, we expect that Tmod could form a 1:1 complex with G-actin in a low salt buffer via the N-terminal G-actin-binding region. Next, after polymerization is initiated by adding salts, a free G-actin interacts with the G-actin already bound to Tmod, forming an "actin dimer." Finally, the C-terminal pointed end-capping region of Tmod binds to the pointed end of the "actin dimer," thereby stabilizing it as a nucleus for polymerization (Fig. 9*C*, *model I*). Alternatively, the C-terminal pointed end-capping region of Tmod may bind to the pointed end of a spontaneously formed actin dimer, independent of the G-actin molecule bound by the N-terminal domain Tmod. Then the three actin molecules bound to Tmod may rearrange and form an actin trimer that is stabilized when Tmod caps its pointed end (Fig. 9*C*, *model II*). Additional experiments will be required to gain more insight into the actin nucleation mechanism by Tmods. Comparison of the G-actin dependence of Tmod-induced polymerization with theoretical models that estimate the largest stable oligomer as a nucleus might provide a clue whether nucleation by Tmods occurs via stabilization of an actin dimer or trimer (61).

Tmods contain two tropomyosin-binding sites (α-helix1 and α-helix3) and one tropomyosin-dependent pointed end-capping site (α-helix2) in their N-terminal domains (Fig. 9*A*) (29). The N-terminal domain can cap tropomyosin-coated actin filament pointed ends independently from the C-terminal domain (20). On the other hand, in our model, the C-terminal but not the N-terminal domain of Tmod predominantly caps the pointed end of an actin nucleus (Fig. 9*C*). Therefore, simultaneous actin nucleation and tropomyosin-dependent pointed end-capping by Tmod may be unlikely. Indeed, disruption of each tropomyosin-binding site by introducing a point mutation in α-helix1 or α-helix3 of Tmod3 has no effect on its actin-nucleating activity (Fig. 7 and data not shown) while completely abolishing its tropomyosin binding and tropomyosin-dependent actin capping activities (29, 30, 44). However, it is possible that tropomyosin could bind to the N-terminal domain of a Tmod whose C-terminal domain caps the pointed end of an actin nucleus, which then may further bind and stabilize actin filament growth from that nucleus.

Do Tmods function as actin nucleators *in vivo*? Although this is still unclear, comparison of actin-nucleating activities among mammalian Tmod isoforms demonstrated that neuronal tissue-specific Tmod2 exhibits the strongest activity, whereas skeletal muscle-specific Tmod4 shows no activity (Fig. 1). Previous studies have shown that dynamic rearrangement of the actin cytoskeleton occurs in neuronal cells to form axons and dendrites (62, 63), whereas actin filaments in mature myofibrils in skeletal muscle are relatively stable (64, 65). Because actin nucleation increases the number of barbed filament ends where polymerization and depolymerization occur, thereby enhancing actin dynamics, these differences in the actin-nucleating activities might be specifically adopted for different actin dynamics in neuronal and muscle cells. In addition to that, we have estimated that the total intracellular concentration of Tmod3 in human microvascular endothelial cells (HMEC-1) is ~0.5 μM (27). There-

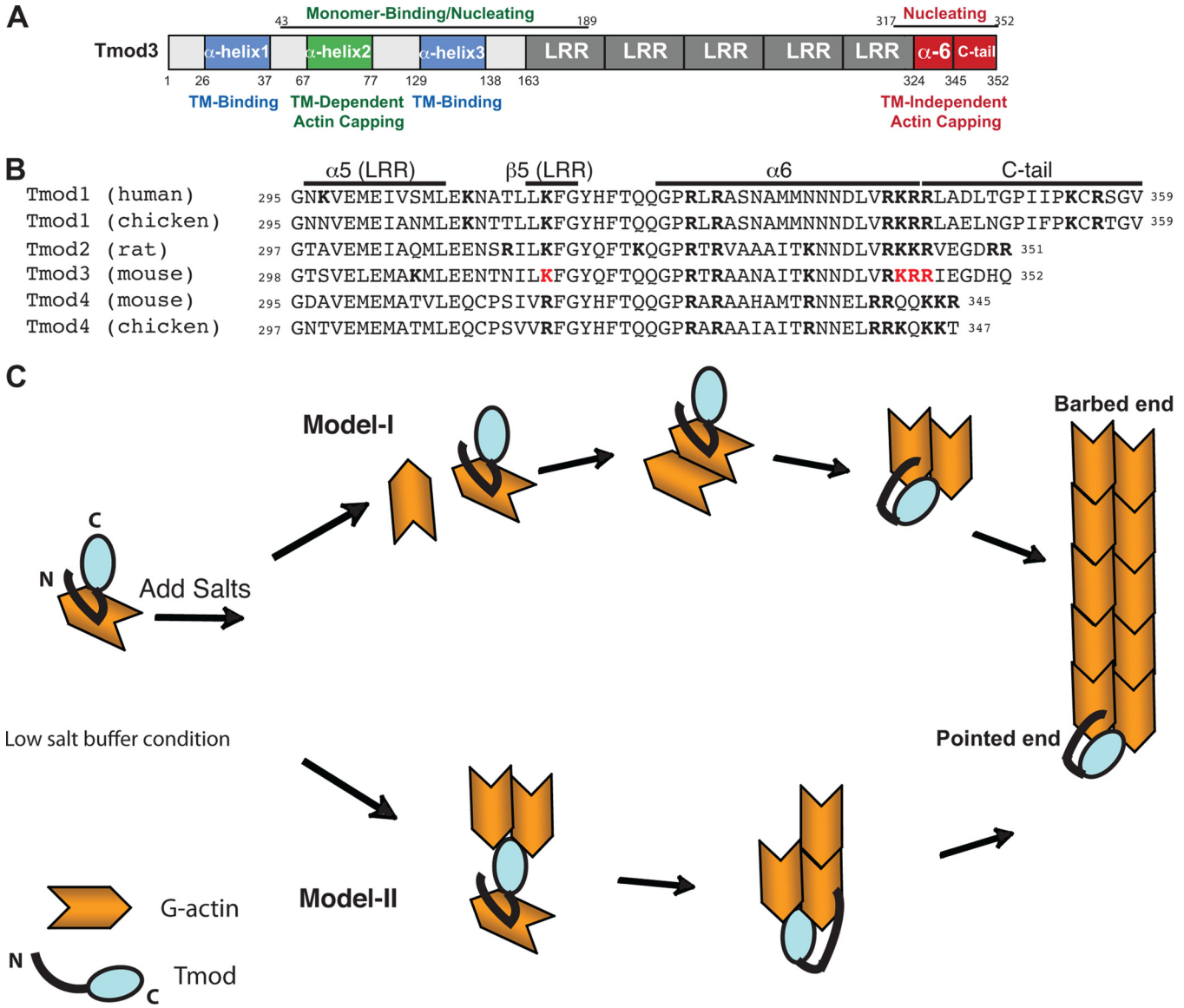

FIGURE 9. **Models for actin nucleation by Tmods.** *A,* schematic diagram of structural domains of Tmod3 based on data from this study and from previous studies on Tmod1 (50). *B,* amino acid sequence comparisons of C termini for various Tmod isoforms 1–4. Basic residues are indicated in *boldface type,* and the residues of mutations for mouse Tmod3 proteins analyzed in Figs. 7–9 are colored in *red.* The first and the last residues indicated for each isoform are numbered. *C,* models for actin nucleation by Tmod1–3. First, Tmod forms a 1:1 complex with G-actin in a low salt buffer via the N-terminal G-actin-binding region. After polymerization is initiated by adding salts, a free G-actin interacts with the G-actin already bound to Tmod, forming an actin dimer, and then the C-terminal pointed end-capping region of Tmod binds to the pointed end of the actin dimer, thereby stabilizing it as a nucleus for polymerization (*model I*). Alternatively, the C-terminal pointed end-capping region of Tmod binds to the pointed end of a spontaneously formed actin dimer, independent of the G-actin molecule bound by N-terminal domain of Tmod. The three actin molecules bound to Tmod rearrange and form an actin trimer that is stabilized when Tmod caps its pointed end (*model II*).

fore, because Tmod3 is expressed ubiquitously (14), sufficient Tmod3 is available to nucleate actin assembly in cells, based on >50 nM concentrations required for actin nucleation *in vitro* (Fig. 1). However, although Tmod3 localizes to lamellipodia in HMEC-1 cells, ectopic expression of GFP-Tmod3 reduces free barbed ends in the lamellipodia, whereas depletion of Tmod3 expression by siRNAi has the opposite effect (27). These observations are inconsistent with actin nucleation by Tmod3 in lamellipodia, which furthermore contain considerably more potent actin nucleators such as Arp2/3 and formins (2, 7). On the other hand, Tmod3 localizes to lateral membranes in human intestinal polarized epithelial Caco-2 cells, and reduction of Tmod3 levels by shRNA leads to a loss of actin filaments from these membranes (26). In this case, Tmod3 may increase the number of actin filaments at lateral membranes by nucleating actin polymerization in Caco2 cells and then stabilize these filaments by capping their pointed ends. Alternatively, the pointed end-capping activity of Tmod3 may be itself sufficient to maintain the concentration of actin filaments on lateral membranes without the additional activity of nucleation. Future cell biological studies with our truncated fragments and point mutants will address which actin-binding properties of Tmods are relevant for their *in vivo* functions, providing tools to uncover clues regarding Tmods' actin regulatory mechanisms in cells.

Acknowledgments—We thank Dr. Takanori Otomo (The Scripps Research Institute), Dr. Dmitri Kudyashov (UCLA), Dr. Emil Reisler (UCLA), Dr. Shoichiro Ono (Emory University), and Dr. Issei Mabuchi (Gakushuin University) for helpful discussions, and Dr. David Gokhin in the Fowler laboratory for help with editing the manuscript. We also thank Jeanette D. Moyer and Zachary L. Wescoe in the Fowler laboratory for technical assistance and Sira Sriswasdi at the Wistar Institute for assistance with software for analysis of cross-linked peptide data.

REFERENCES

1. Pollard, T. D., Blanchoin, L., and Mullins, R. D. (2000) *Annu. Rev. Biophys. Biomol. Struct.* **29,** 545–576
2. Le Clainche, C., and Carlier, M. F. (2008) *Physiol. Rev.* **88,** 489–513
3. Jackman, M. R., Shurety, W., Ellis, J. A., and Luzio, J. P. (1994) *J. Cell Sci.* **107,** 2547–2556
4. Stevenson, B. R., and Begg, D. A. (1994) *J. Cell Sci.* **107,** 367–375
5. Dubin-Thaler, B. J., Hofman, J. M., Cai, Y., Xenias, H., Spielman, I., Shneidman, A. V., David, L. A., Döbereiner, H. G., Wiggins, C. H., and Sheetz, M. P. (2008) *PLoS One* **3,** e3735
6. Qualmann, B., and Kessels, M. M. (2009) *Trends Cell Biol.* **19,** 276–285
7. Pollard, T. D. (2007) *Annu. Rev. Biophys. Biomol. Struct.* **36,** 451–477
8. Ahuja, R., Pinyol, R., Reichenbach, N., Custer, L., Klingensmith, J., Kessels, M. M., and Qualmann, B. (2007) *Cell* **131,** 337–350
9. Zuchero, J. B., Coutts, A. S., Quinlan, M. E., Thangue, N. B., and Mullins, R. D. (2009) *Nat. Cell Biol.* **11,** 451–459
10. Quinlan, M. E., Heuser, J. E., Kerkhoff, E., and Mullins, R. D. (2005) *Nature* **433,** 382–388
11. Chereau, D., Boczkowska, M., Skwarek-Maruszewska, A., Fujiwara, I., Hayes, D. B., Rebowski, G., Lappalainen, P., Pollard, T. D., and Dominguez, R. (2008) *Science* **320,** 239–243
12. Goley, E. D., and Welch, M. D. (2006) *Nat. Rev. Mol. Cell Biol.* **7,** 713–726
13. Pruyne, D., Evangelista, M., Yang, C., Bi, E., Zigmond, S., Bretscher, A., and Boone, C. (2002) *Science* **297,** 612–615
14. Conley, C. A., Fritz-Six, K. L., Almenar-Queralt, A., and Fowler, V. M. (2001) *Genomics* **73,** 127–139
15. Wen, K. K., Rubenstein, P. A., and DeMali, K. A. (2009) *J. Biol. Chem.* **284,** 30463–30473
16. Fischer, R. S., and Fowler, V. M. (2003) *Trends Cell Biol.* **13,** 593–601
17. Cox, P. R., and Zoghbi, H. Y. (2000) *Genomics* **63,** 97–107
18. Almenar-Queralt, A., Lee, A., Conley, C. A., Ribas de Pouplana, L., and Fowler, V. M. (1999) *J. Biol. Chem.* **274,** 28466–28475
19. Weber, A., Pennise, C. R., Babcock, G. G., and Fowler, V. M. (1994) *J. Cell Biol.* **127,** 1627–1635
20. Fowler, V. M., Greenfield, N. J., and Moyer, J. (2003) *J. Biol. Chem.* **278,** 40000–40009
21. Fritz-Six, K. L., Cox, P. R., Fischer, R. S., Xu, B., Gregorio, C. C., Zoghbi, H. Y., and Fowler, V. M. (2003) *J. Cell Biol.* **163,** 1033–1044
22. Gokhin, D. S., Lewis, R. A., McKeown, C. R., Nowak, R. B., Kim, N. E., Littlefield, R. S., Lieber, R. L., and Fowler, V. M. (2010) *J. Cell Biol.* **189,** 95–109
23. Mudry, R. E., Perry, C. N., Richards, M., Fowler, V. M., and Gregorio, C. C. (2003) *J. Cell Biol.* **162,** 1057–1068
24. Littlefield, R. S., and Fowler, V. M. (2008) *Semin. Cell Dev. Biol.* **19,** 511–519
25. Nowak, R. B., Fischer, R. S., Zoltoski, R. K., Kuszak, J. R., and Fowler, V. M. (2009) *J. Cell Biol.* **186,** 915–928
26. Weber, K. L., Fischer, R. S., and Fowler, V. M. (2007) *J. Cell Sci.* **120,** 3625–3632
27. Fischer, R. S., Fritz-Six, K. L., and Fowler, V. M. (2003) *J. Cell Biol.* **161,** 371–380
28. Greenfield, N. J., Kostyukova, A. S., and Hitchcock-DeGregori, S. E. (2005) *Biophys. J.* **88,** 372–383
29. Kostyukova, A. S., Choy, A., and Rapp, B. A. (2006) *Biochemistry* **45,** 12068–12075
30. Kostyukova, A. S., Rapp, B. A., Choy, A., Greenfield, N. J., and Hitchcock-DeGregori, S. E. (2005) *Biochemistry* **44,** 4905–4910
31. Fischer, R. S., Yarmola, E. G., Weber, K. L., Speicher, K. D., Speicher, D. W., Bubb, M. R., and Fowler, V. M. (2006) *J. Biol. Chem.* **281,** 36454–36465
32. Paavilainen, V. O., Bertling, E., Falck, S., and Lappalainen, P. (2004) *Trends Cell Biol.* **14,** 386–394
33. Kuipers, O. P., Boot, H. J., and de Vos, W. M. (1991) *Nucleic Acids Res.* **19,** 4558
34. Babcock, G. G., and Fowler, V. M. (1994) *J. Biol. Chem.* **269,** 27510–27518
35. Pardee, J. D., and Spudich, J. A. (1982) *Methods Cell Biol.* **24,** 271–289
36. Kouyama, T., and Mihashi, K. (1981) *Eur. J. Biochem.* **114,** 33–38
37. Bryan, J. (1988) *J. Cell Biol.* **106,** 1553–1562
38. Young, C. L., Southwick, F. S., and Weber, A. (1990) *Biochemistry* **29,** 2232–2240
39. Pollard, T. D. (1986) *J. Cell Biol.* **103,** 2747–2754
40. Laemmli, U. K. (1970) *Nature* **227,** 680–685
41. Safer, D. (1989) *Anal. Biochem.* **178,** 32–37
42. Speicher, K. D., Kolbas, O., Harper, S., and Speicher, D. W. (2000) *J. Biomol. Tech.* **11,** 74–86
43. Campellone, K. G., and Welch, M. D. (2010) *Nat. Rev. Mol. Cell Biol.* **11,** 237–251
44. Kong, K. Y., and Kedes, L. (2006) *J. Biol. Chem.* **281,** 9589–9599
45. Kostyukova, A. S., Hitchcock-Degregori, S. E., and Greenfield, N. J. (2007) *J. Mol. Biol.* **372,** 608–618
46. Kostyukova, A. S., Tiktopulo, E. I., and Maéda, Y. (2001) *Biophys. J.* **81,** 345–351
47. Krieger, I., Kostyukova, A. S., and Maéda, Y. (2001) *Acta Crystallogr. D. Biol. Crystallogr.* **57,** 743–744
48. Fujisawa, T., Kostyukova, A., and Maéda, Y. (2001) *FEBS Lett.* **498,** 67–71
49. Marekov, L. N. (2007) *Curr. Protoc. Protein Sci.* **47,** 19.16.1–19.16.8
50. Krieger, I., Kostyukova, A., Yamashita, A., Nitanai, Y., and Maéda, Y. (2002) *Biophys. J.* **83,** 2716–2725
51. Goode, B. L., and Eck, M. J. (2007) *Annu. Rev. Biochem.* **76,** 593–627
52. Mahaffy, R. E., and Pollard, T. D. (2006) *Biophys. J.* **91,** 3519–3528
53. Paul, A. S., and Pollard, T. D. (2009) *Cell Motil. Cytoskeleton* **66,** 606–617
54. Caldwell, J. E., Heiss, S. G., Mermall, V., and Cooper, J. A. (1989) *Biochemistry* **28,** 8506–8514
55. Schafer, D. A., Jennings, P. B., and Cooper, J. A. (1996) *J. Cell Biol.* **135,** 169–179
56. Cooper, J. A., and Pollard, T. D. (1985) *Biochemistry* **24,** 793–799
57. Mannherz, H. G., and Hannappel, E. (2009) *Cell Motil. Cytoskeleton* **66,** 839–851
58. Safer, D., Sosnick, T. R., and Elzinga, M. (1997) *Biochemistry* **36,** 5806–5816
59. Domanski, M., Hertzog, M., Coutant, J., Gutsche-Perelroizen, I., Bontems, F., Carlier, M. F., Guittet, E., and van Heijenoort, C. (2004) *J. Biol. Chem.* **279,** 23637–23645
60. Irobi, E., Aguda, A. H., Larsson, M., Guerin, C., Yin, H. L., Burtnick, L. D., Blanchoin, L., and Robinson, R. C. (2004) *EMBO J.* **23,** 3599–3608
61. Pring, M., Evangelista, M., Boone, C., Yang, C., and Zigmond, S. H. (2003) *Biochemistry* **42,** 486–496
62. Witte, H., and Bradke, F. (2008) *Curr. Opin. Neurobiol.* **18,** 479–487
63. Geraldo, S., and Gordon-Weeks, P. R. (2009) *J. Cell Sci.* **122,** 3595–3604
64. Sanger, J. M., Mittal, B., Wegner, A., Jockusch, B. M., and Sanger, J. W. (1987) *Eur. J. Cell Biol.* **43,** 421–428
65. Wang, J., Sanger, J. M., and Sanger, J. W. (2005) *Cell Motil. Cytoskeleton* **62,** 35–47
66. Weber, A., Pennise, C. R., and Fowler, V. M. (1999) *J. Biol. Chem.* **274,** 34637–34645
67. Schutt, C. E., Myslik, J. C., Rozycki, M. D., Goonesekere, N. C., and Lindberg, U. (1993) *Nature* **365,** 810–816
68. Moyer, J. D., Nowak, R. B., Kim, N. E., Larkin, S. K., Peters, L. L., Hartwig, J., Kuipers, F. A., and Fowler, V. M. (2010) *Blood*, in press